JOURNAL OF THE AERONAUTICAL SCIENCES

VOLUME 9 SEPTEMBER, 1942 NUMBER 11

Tricycle Landing Gear Design—Part 2*

E. S. JENKINS AND A. F. DONOVAN
Curtiss-Wright Corporation

Nose Wheel Design

General

IN THE DEVELOPMENT of a nose wheel installation, the designer is confronted with the problems of eliminating shimmy, obtaining satisfactory maneuverability and ground-handling characteristics, providing adequate structural strength, and coordinating wheel size and location with the airplane geometry and structure. These problems are closely interrelated, and it is impossible to give exact criteria covering all the factors involved in obtaining the most satisfactory installation. Enough is known about the various characteristics, however, to provide the information necessary to produce a workable solution. Usually, the nose wheel size and type can be selected on the basis of the structural loads and space requirements. The tire size can be chosen to give low enough ground pressure to prevent burying; the trail can be determined from considerations of ground handling and wheel size; the caster angle is best fixed on the basis of structural, geometric, and ground-handling requirements; and the shimmy can then be prevented by the provision of damping adequate for the characteristics of the system. The damping required, however, is determined by the type of tire, caster angle, trail, and moment of inertia of the rotating assembly so that consideration should also be given in determining these items to their effect on the tendency to shimmy. For this reason, the problem of eliminating shimmy will be considered first so that in studying the other requirements their relationship to the shimmy problem can be considered.

Prevention of Shimmy

Theory of Shimmy

All rubber-tired castering wheels tend to shimmy. The reasons for this can be found by studying the action of a castering wheel when the spindle or caster axis is moved along a straight path and the wheel is started from a position at an angle to this path.

In the initial position shown in Fig. 11, the centerline of the tire periphery in the contract area is a straight line and lies below the centerline of the wheel fork, which is at an angle, θ, to the path along which the caster axis is to be moved. Initially, there is neither side load nor twist on the tire. The moment about the caster axis must be zero, of course, since it is a free swiveling joint, and this condition is satisfied by neither side forces nor torque from the ground contact area.

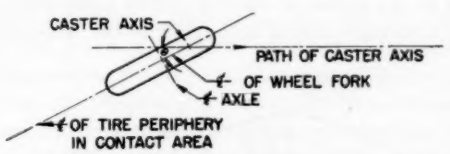

FIG. 11. Condition of wheel and tire at beginning of motion

If, now, the caster axis is moved along its path a short distance, the tire will move along the path of the centerline of the tire periphery in the contact area at the angle θ to the path of the caster axis. The wheel fork will swivel about the caster axis slightly to account for the amount that the centerline of the wheel has moved toward the caster axis path. However, the friction between the tire tread and the ground will keep the contact area from turning to line up with the wheel fork. The centerline of the wheel fork will then be at an angle to the centerline of the tire periphery in the contact area so that the wheel fork will be pulling with a sidewise component on the wheel contact area.

The tire is thus deflected sideways and twisted between the axle and the tread at the point of ground contact as shown in Fig. 12. Being an elastic body, the tire requires a torque and a side force at the contact

Copyright, 1942, by E. S. Jenkins and A. F. Donovan.

* Continued from the August issue, pp. 385–396.

area to deflect it in this manner. The moment about the castering axis must be zero, however, or the fork would turn, so the moment of the side force about the caster axis must be equal to the ground torque. That is,

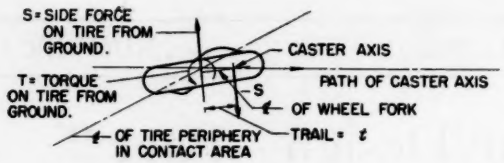
S = SIDE FORCE ON TIRE FROM GROUND.
CASTER AXIS
T = TORQUE ON TIRE FROM GROUND.
PATH OF CASTER AXIS
S
OF WHEEL FORK
℄ OF TIRE PERIPHERY IN CONTACT AREA
TRAIL = t

FIG. 12. Condition of wheel and tire after moving a short distance.

$$St - T = 0 \tag{44}$$

If the caster axis were moved still farther along the course and if the tire tread were continued along its initial path, the ground forces would soon become greater than the frictional restraint and the tire would skid around. Actually, as soon as the tire is deflected sidewise or twisted, the peripheral centerline is distorted into a curve instead of the original straight line. Consider the case of a tire deflected sidewise only. The projection of the lower half of the peripheral centerline on the ground would resemble Fig. 13, showing the tire as it would look from below. It can be seen that the peripheral centerline in the region of contact has become a curve so that the tire tread is approximately following a circle of radius R. If the tire were only twisted, the peripheral centerline would resemble Fig. 14. Here, the peripheral centerline is an S curve which in the region of contact can be considered effectively a straight line at an angle θ to the wheel centerline.

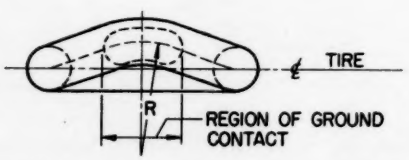

FIG. 13. Bottom view of a tire resisting a lateral ground force.

FIG. 14. Bottom view of a tire resisting a ground torque.

If the tire is both twisted and deflected sideways, the peripheral centerline will have a shape corresponding to the sum of the two effects. In the region of contact this would be an arc turned through an angle θ with reference to the centerline of the tire and displaced sideways a distance λ as shown in Fig. 15. It is easily seen that the radius of curvature of the arc is determined by the displacement λ. If λ is zero, the contact centerline is effectively straight. As λ increases, the contact centerline becomes more and more curved—concave toward the undisplaced tire center.

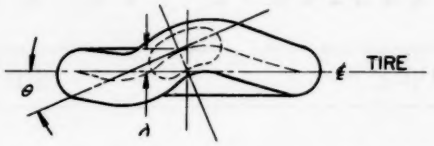

FIG. 15. Bottom view of a tire resisting both a lateral force, and a torque from the ground.

Returning now to the problem of the motion of the castering wheel, it is apparent that after the caster axis has moved ahead a short distance and the tire has been bent sideways and twisted the peripheral centerline in contact with the ground will be an arc instead of a straight line. The tire tread will follow this arc that is curving toward the caster axis. At the instant of starting forward, the contact centerline is a straight line. As the tire rolls forward and is deflected sideways, the contact centerline becomes increasingly curved with the tire deflection. The path of the tire centerline will, therefore, be approximately as shown in Fig. 16, together with the positions of the fork centerline and caster axis.

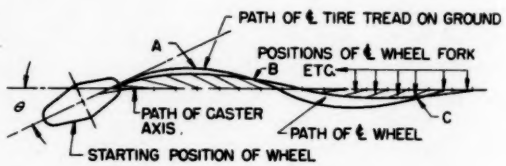

FIG. 16. Kinematic shimmy.

Because of the curvature of the arc of the contact centerline, the tire tread does not continue on its original path at the angle θ but turns slowly toward the path of the caster axis. It does not become parallel to the caster axis path, however, until well after it has crossed the path. When the tire contact centerline does become approximately parallel to the caster axis path at point A of Fig. 16, the centerline of the wheel fork is at an angle to the caster axis path and the tire is still deflected sideways and twisted. The sidewise displacement is the distance between the centerline of the wheel and the centerline of the tire tread, and the angle of twist of the tire is the angle between the centerline of the wheel fork and a tangent to the path of the centerline of the tire tread at the corresponding point. In the figures, of course, angles and deflections have been exaggerated to illustrate the action. Because of the displacement of the tread with relation to the wheel centerline at the point A, the contact centerline is still an arc and the tire will continue to follow a curved path even though a tangent at the middle of the tire contact

centerline is parallel to the path of the caster axis. This curved path will bring it to point B. At point B the tire contact centerline has curved around sufficiently so that it lines up with the centerline of the wheel fork. The angle of twist of the tire and the twisting torque from the ground are therefore zero. Likewise, the centerline of the wheel is directly over the centerline of the contact area, so the sidewise displacement and side load are zero and the contact centerline is a straight line instead of an arc. The wheel fork centerline, however, is at an angle to the path of the caster axis. The condition is thus exactly the same as that at the starting position of the wheel, except that the wheel is on the opposite side of the caster axis path. The actions just described would, therefore, be repeated, but with displacements and angles of opposite sign to those of the first part of the cycle. When the tire reaches the point C, the condition is exactly the same as at the starting position. Therefore, further movement of the caster axis would only repeat the previous motions.

Thus, a rubber-tired, freely castering wheel will oscillate from side to side when the caster axis is moved along a straight path at an angle to the original tire position. This phenomenon is known as kinematic shimmy. The maximum possible amplitude of this type of shimmy is limited by the friction between the tire and the ground. Obviously, if the displacements and angles get very large, the tire tread will skid on the ground until the tire more nearly lines up with the caster axis path. Pure kinematic shimmy is, therefore, limited in magnitude and, by itself, would not be serious enough to interfere with the proper functioning of a nose wheel.

Unfortunately, there are other effects that must be considered in a complete analysis of the problem. Roughly, the action may be described as follows. If a mass, such as an airplane, supported on rubber tires is pushed sideways and then released, it will vibrate sideways at a frequency determined by the effective spring constant of the tire. Likewise, if a *freely* castering wheel of considerable mass and supporting an appreciable load is twisted about its caster axis and then released the wheel will vibrate torsionally at a frequency determined by the moment of inertia of the wheel about the castering axis and the effective torsional spring constant of the tire. In both of these cases the tire friction on the ground must be greater than the applied forces.

Consider now a castering wheel with an appreciable moment of inertia about the castering axis executing the kinematic shimmy as previously described. At extremely low speeds the conditions will be exactly similar. As the forward speed increases, and with it the frequency of the kinematic shimmy, the period of oscillation will become closer and closer to the natural torsional period of the wheel. The forces acting on the tire due to the kinematic shimmy will then produce a forced vibration or dynamic shimmy of the wheel, increasing in amplitude as the frequency becomes nearer to the natural frequency of the wheel. The vibration results in a greater twist and displacement of the tire than was the case in the kinematic shimmy, so that with each successive cycle the amplitude becomes greater and the oscillation more violent. This is particularly true when the frequency of the kinematic shimmy coincides with the resonant torsional frequency of the castering wheel. At resonance, only small pulsating forces are necessary to produce an infinite amplitude of oscillation. As the amplitude is measured by the angle of the centerline of the wheel fork to the caster axis path, this condition may be said to be realized when the wheel makes complete revolutions about the castering axis, a phenomenon that has been frequently observed on undamped castering wheels.

The castering wheel and tire thus form a vibrating system with 2 degrees of freedom, lateral deflection of the tire, and twisting of the tire between the ground and the wheel axle. The kinematic shimmy, meanwhile, provides lateral and twisting forces on the tire at a frequency proportional to the forward speed. Whenever the period of the kinematic forces approaches that of the vibrating system, the dynamic shimmy will become extremely violent. The vibrating system is the result of the spring actions of the tire and the mass of the wheel and cannot be eliminated so long as a pneumatic tire is used. The kinematic shimmy is the result of the tire flexibility and the characteristic of a tire that, when deflected sideways, the peripheral centerline becomes an arc concave toward its undeflected position. Therefore, any tire except one rigid laterally or torsionally will tend to shimmy.

On the basis of the description of castering wheel shimmy just given, a complete mathematical analysis giving amplitudes, frequencies, divergences, and other information can be made if the necessary characteristics of the system are known. The data required are the lateral and torsional spring constants of the tire, the radius of curvature of the peripheral contact centerline for a unit lateral deflection of the tire, and the moment of inertia of the wheel and other castering parts about the caster axis. Such analyses have been made by Wylie,[3] Kantrowitz,[4] and Taylor.[5] In these analyses an additional factor, the effect of tire angle of twist on the radius of curvature of the contact centerline, which was neglected in the previous discussion is included. The general theory remains the same, the difference being that in Fig. 15 the radius of curvature of the contact centerline is inversely proportional to the lateral deflection λ times a function of the angle θ, instead of to λ alone.

Any vibration can be stopped by providing a damping device that will absorb more energy at all possible amplitudes of vibration than is fed into the system by the exciting forces. Methods of calculating the amount of damping required are developed from the mathematical theory in the references mentioned above.

It should be remembered that throughout the previous shimmy description the caster axis has been forced to follow a straight path and resist the side load produced on the tire. Obviously, on an actual airplane the reacting force must arise from the inertia of the airplane. Therefore, at extremely low frequencies and speed the inertia force is negligible, the caster axis is free to move sideways, and the kinematic shimmy cannot be produced. As the speed increases, the resistance of the airplane to lateral movement increases accordingly, so that in the usual range of frequencies the resistance is so great that the assumption that the caster axis follows a straight path produces a negligible error. This problem has been solved analytically by Kantrowitz[4] and Wylie.[3]

The effect of the lateral restraint of the caster axis on the shimmy suggests that the shimmy might be eliminated by changing the characteristics of the system to eliminate the coupling between the 2 degrees of freedom. This amounts to disconnecting the exciting forces from the torsional system. Two methods of doing this have been proposed and tried experimentally.[4] Basically, both methods make it possible for the wheel to shift freely sideways without also rotating about the caster axis. Thus, it is impossible for any side force to build up on the tire to cause it to shimmy. The first method of providing this freedom is to leave a certain amount of clearance on each side of the wheel so it can slide sideways on the axle. The axle is bowed slightly to provide a tendency to keep the wheel centered on the axle. This method was tried by the N.A.C.A. on the Weick, W-1 airplane and proved satisfactory so long as the maximum angle of rotation of the castering spindle was limited to ± 13 deg. Other tests have not usually supported this theory, probably because the friction on the axle was too great, but possibly because the mass of the wheel was sufficient for its inertia forces to provide the necessary lateral restraint. The second method suggested for providing lateral freedom is to use two castering axes, one in front of the other, connected by an intermediate link as shown by Fig. 17.

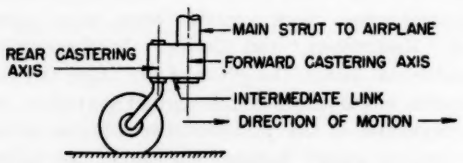

FIG. 17. Double spindle castering wheel.

The N.A.C.A. tested this system in the laboratory and found that it eliminated shimmy. The method has also been studied by E. R. Warner.[6] The action of the system is obvious. No side load and torque can be built up on the wheel, since in accordance with Eq. (44) the moment would have to be zero about both castering axes at the same time—an impossible condition. This system would seem to be more practical than the sliding axle system for actual use, although the structural complications are considerable and retracting difficulties would be increased. It might be possible, however, if such an arrangement would satisfactorily eliminate shimmy, to design it to be as light as a damped system. The elimination of the adverse effects of the damping friction on steering and ground handling and the removal of the necessity of servicing a dampener would be worth-while advantages. A partial compensation for the structural complications of the link would be the elimination of the scissors usually used to transfer the shimmy torque to the dampener.

Damping

The only means of preventing shimmy in use on airplanes at present is damping of some type. The other methods mentioned previously have either been found unsatisfactory under service operating conditions or have never been subjected to full scale tests. Therefore, the remainder of this section on shimmy prevention is devoted to the study of damping and dampeners and covers the effects of various factors on the amount of damping required, calculation of the damping necessary to produce a converging oscillation, kinds of damping, and types of dampeners.

Factors Affecting Damping Requirements

The factors affecting the damping requirements are the tire characteristics, moment of inertia of the castering parts about the caster axis, trail, and caster angle. It is obvious from the theory of shimmy previously developed that except for the caster angle, which was considered zero, these items are the determining factors. That the caster angle will also affect the shimmy is apparent from the consideration that with caster angles other than zero the torque from the tire must be broken up into components parallel and perpendicular to caster axis before using it in Eq. (44). Of the factors controlling the shimmy, the tire properties and castering moment of inertia are the most important, the trail and caster angle having a lesser effect.

The tire characteristics involved in the determination of the damping requirements were mentioned briefly earlier in the paper. Values of tire constants were measured by Howard[7] for streamline, low-pressure, and air wheel tires of approximately 16-in. diameter. These values were extended on the basis of geometric similarity and inserted in equations developed by Kantrowitz[4] to give general formulas for the amount of viscous damping necessary to prevent shimmy in terms of the tire radius and moment of inertia of the castering parts. These formulas are tabulated below:

Air wheel tire	$K_{max.} = 0.28r^2\sqrt{I_w}$	(45)
Low-pressure tire	$K_{max.} = 0.45r^2\sqrt{I_w}$	(46)
Streamline tire	$K_{max.} = 0.56r^2\sqrt{I_w}$	(47)

The damping, $K_{max.}$, is in terms of ft.lbs. per deg. per sec.; the tire radius, r, is in ft.; and the moment of inertia I_w, is in slug ft. sq. These formulas are for zero caster angle and trail. No information is available as to their accuracy, but it seems probable that they satisfactorily indicate the relative amounts of damping required by the different types of tires. Thus, a streamline tire requires twice the viscous damping of an air wheel tire and 24 per cent more than a low-pressure tire. In general, variations in tire pressure or load have a negligible effect on viscous damping requirements.

It is obvious from the above formulas that the damping required is proportional to the square root of the moment of inertia of the castering parts and also that it varies as the square of the tire diameter. The moment of inertia, however, is approximately proportional to the fourth power of the tire diameter so that, approximately, the damping required increases with the square root of the fourth power times the second power, or as the fourth power of the tire diameter.

Experimental data on the effect of trail on the damping requirements is given by Howard.[7] In general, for the usual amounts of trail the tendency to shimmy becomes slightly greater with increase in trail. Wylie[3] develops an analytic relationship for the effect of trail, but it is too complicated to be easily applied.

A graph of caster angle coefficient is given by Wylie[3] based on experimental data on model tires reported by Kantrowitz.[4] A study of the analytic development of the damping equations shows that the viscous damping required is proportional to the square root of the caster angle coefficient. The damping required for a given caster angle, therefore, is equal to the damping for zero caster angle, as computed by the formulas above, times the square root of the ratio of caster angle coefficient for the given caster angle to that for zero caster angle. Values of the square root of this ratio are plotted in Fig. 18 against caster angle, and the amount of damping for a given caster angle relative to that for zero caster angle can thus be read directly from the curve. The damping required increases with positive (caster axis sloping aft from the wheel) caster angle and, although it is not shown on the curve, experimental evidence given by Howard[7] indicates that it decreases with negative caster angles down to −8 deg. and, beyond this, slowly increases.

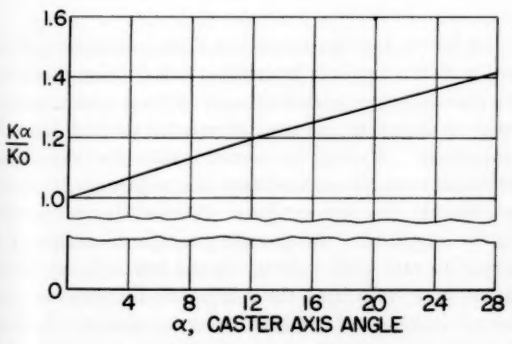

FIG. 18. Effect of caster angle on viscous damping requirements.

Tire Constants

In the previous section the general effect of various factors on the amount of viscous damping required to prevent shimmy has been given together with approximate formulas for computing it. However, because of the scanty data on which these formulas are based, it is advisable to determine the tire constants experimentally for the tire under consideration with the values of trail and caster angle with which it is to be used. These tire constants can then be inserted in the damping formula developed by Kantrowitz[4] and the damping requirements can be determined. This will eliminate the errors introduced in Eqs. (45) through (47) by assuming the tire constants functions of the tire radius and, in addition, will account for the effects of trail and caster angle.

There are four tire constants to be determined. Three of these are essential to any calculations on shimmy, but the fourth is required only if the effect of lateral motion of the airplane is to be taken into account. The three basic constants are:

1. K_1, the curvature of the tire peripheral centerline in the contact area for a unit lateral deflection of the load point and no torsional restraint at the caster axis.

2. $C_1 I_w$, the torque about the caster axis necessary to make the tire roll along a path at a constant angle θ to the wheel centerline with a unit lateral deflection of the load point from the wheel centerline.

3. C_2, the angle between the contact centerline and the path of travel, at unit lateral deflection of the load point, when the tire has been given a lateral deflection and the wheel made to roll straight along the path of its centerline extended.

The fourth constant is usually neglected in the calculations since it has a negligible effect on the damping except at low forward speeds; it is E_λ, the lateral force at the ground necessary to produce unit lateral deflection of the tire. These constants may be measured by the methods described by Howard.[7]

Calculation of Viscous Damping from Tire Constants

The damping necessary to prevent shimmy is a function of the forward speed; this is apparent from the discussion given in the section on the theory of shimmy. At the velocity requiring the maximum damping, $K_{max.}$, the value is given by Kantrowitz[4] as

$$K_{max.} = I_w \sqrt{\frac{C_1 C_2}{K_1}} \left(\sqrt{1 + \frac{K_1}{C_2^2}} - 1 \right) \qquad (48)$$

In using Eq. (48) the units must be consistent. That is, if the constants were determined in units of lbs., ft., and

ft.lbs., the moment of inertia should be in slug ft. sq., and the damping will be in ft.lbs. per rad. per sec.

Kantrowitz[4] also determines the speed at which this damping is necessary as

$$V_0 = \sqrt{C_1/C_2K_1} \tag{49}$$

This result will be in ft. per sec. if the constants are in the same units as listed above.

Kinds of Damping

Throughout the previous discussion on the elimination of shimmy by damping, only viscous damping was mentioned. In practice, pure viscous damping is never used in actual shimmy dampeners since it would require an excessively large dampener. Actual dampeners usually use either dry friction damping or hydraulic damping, in which a fluid is forced through an orifice. In the mathematical development of the damping formulas, it was necessary to express the damping torque in terms of the angular velocity of the shimmy. The resulting differential equation has a simple analytic solution only when the damping torque is assumed to be directly proportional to the angular velocity. Damping, which is directly proportional to velocity, is known as pure viscous friction damping. Physically, this type of damping is approximated by a thin flat plate arranged to move edgewise through a viscous fluid.

Dry or solid friction damping is usually considered mathematically to provide a constant damping force or torque independent of velocity. As described by its name, such a dampener usually uses dry friction to obtain the damping torque. Actually, damping produced in this manner is usually a maximum at zero velocity, decreasing somewhat as soon as motion begins and remaining substantially constant for further increases in velocity.

Hydraulic or turbulent fluid friction damping is described mathematically as producing resisting forces proportional to the square of the velocity. This type of damping is approximated by a flat plate arranged to supply the damping force by moving broadside through a fluid of low viscosity or by a system that forces a low viscosity fluid through an orifice.

Spring-loaded, pressure relief valves are sometimes used in hydraulic dampeners, usually in addition to a small plain orifice. The spring-loaded valve remains closed until sufficient fluid pressure is built up to overcome the spring. The opening of the valve increases the total orifice area and thus prevents the torque from increasing as the velocity squared. By suitable design of the valve and valve spring, a wide variety of damping characteristics may be obtained. In general, for shimmy damping, satisfactory characteristics can be obtained by using an oil of medium viscosity forced through a simple orifice and by omitting the extra complications of a relief valve.

Because of the lack of a direct analytic solution for problems involving other than pure viscous damping, it is customarily assumed that if another type of damping takes an amount of energy out of an oscillation equal to the energy taken out by a given amount of viscous damping it is equivalent to that amount of viscous damping for the purpose of damping the oscillation. This assumption usually gives satisfactory results for the types of damping generally encountered in practice. Therefore, if the amount of viscous damping necessary is known, the energy that must be absorbed from the vibrating system per cycle can be calculated. Accordingly, a dampener using other than pure viscous friction but with the same energy capacity can be selected.

In actual fluid dampeners the damping force or torque varies with the amplitude of the oscillation as well as with the instantaneous velocity. In addition, it is usually possible, by adjusting an orifice valve or pressure relief valve spring, to alter the characteristics over a considerable range. Manufacturers usually give the dampener characteristics as curves of torque against angular velocity for several different amplitudes at particular control-valve settings. The general shape of these curves with the control valve set one-quarter closed is shown by Fig. 19. It is immediately apparent that they

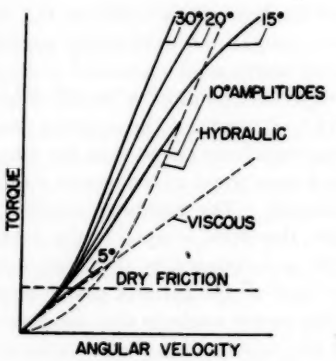

FIG. 19. Typical hydraulic dampener characteristics.

do not follow any mathematical laws as simple as those used to define viscous, hydraulic, and friction damping. The characteristic curves of each of these mathematical types of damping are also shown by dotted lines for comparison. It will be noticed that for the 5-deg. amplitude and correspondingly low velocities the curve corresponds to almost pure viscous damping. For greater amplitudes the damping torque increases at an increasing rate with velocity in the low-velocity range, but at high velocities the curvature reverses and the rate of increase of torques becomes smaller with increased velocity. The general effect of closing the control valve is to steepen the curves and reduce the upward curvature near the origin. Thus, for the lower angular velocity range in which the dampener actually operates, closing the valve tends to make the damping less of the hydraulic type and more nearly of the viscous type, as well as increasing the amount of damping.

For a dampener with characteristics of this type it can be readily determined whether shimmy will be theoretically eliminated in an installation by plotting the required viscous damping as determined by the theory on the same graph with the dampener characteristics. As the viscous damping is given in terms of torque per unit angular velocity, this is a straight line passing through the origin with a slope equal to the calculated damping. It is apparent from the shape of the curves in the graph that the greatest probability of shimmy is at small angular velocities and, of course, correspondingly low amplitudes. If the required viscous damping line is tangent to the actual dampener characteristics at zero velocity, the dampener will be the minimum size necessary to produce a converging oscillation. This case is illustrated by Fig. 19. If the slope of the required damping line is less than that of the dampener at zero velocity, the dampener is more than sufficient to eliminate the shimmy. On the other hand, if the required damping line is steeper than the dampener characteristics at zero velocity so that more torque is required at low velocities than the dampener can supply, the wheel will shimmy. In addition, if the required damping line crosses the dampener characteristic curves at a higher velocity so that above this velocity the dampener supplies more torque than is necessary, then the shimmy will be limited to a maximum amplitude where the energy absorbed by the excess over the required viscous torque during the high velocity part of the cycle just compensates for the deficiency in energy absorption during the low-velocity part of the cycle. If the required viscous damping line is above all the dampener curves, the shimmy will not be limited in amplitude by the dampener. The only satisfactory method in practice is to eliminate completely the shimmy, since even extremely small amplitudes are undesirable. In addition, the damping equation holds only for small shimmy amplitudes and assumes that the tire does not skid. Therefore, if insufficient damping is provided to eliminate completely the shimmy, the amplitude developed may be sufficient to alter the shimmy conditions so that the shimmy will continue to build up instead of reaching an equilibrium amplitude. It has also been found desirable in some cases to use a greater degree of damping than the minimum that will produce a converging oscillation, in order to damp out any disturbance in a single oscillation.

Certain conclusions concerning other kinds of damping can be drawn from Fig. 19. Dry friction damping, for example, has an excess of torque over viscous damping at low angular velocities, has the same torque at an intermediate velocity, and is deficient in torque at higher velocities. Thus, from Fig. 19, as long as the maximum velocity during a cycle did not exceed that where the viscous damping line crossed the dry friction line, the friction dampener would be absorbing more energy throughout the entire cycle than that required to prevent shimmy. If the maximum velocity is greater than that at the line intersection, then during the portion of the cycle when the velocity is above this value the friction dampener will be absorbing less energy than the viscous dampener. The friction dampener will then prevent shimmy so long as the excess energy absorbed during the low-speed part of the cycle is greater than the deficiency during the high-speed part. Obviously, as the maximum velocity of the cycle is increased, the energy deficiency for the faster part will increase also, so that a velocity will be reached where the high-speed deficiency becomes greater than the low-speed excess. If the wheel starts to shimmy at velocities in excess of this value, the shimmy will increase in amplitude; at velocities below this value it will be damped out. The maximum velocity during a cycle is determined by the frequency and amplitude of the shimmy. As discussed under "Theory of Shimmy" (Part 2), there is a certain frequency requiring the most damping. Therefore, for this frequency there is a certain maximum amplitude at which the frictional dampener will prevent shimmy. If the wheel strikes the ground at an angle to its path greater than this maximum amplitude, it will shimmy. Likewise, if it hits an obstruction that turns it through a sufficient angle, it will shimmy.

Fortunately, there is an exception to this. If the angle is sufficient to cause the tire to skid, the skidding friction between the tire and ground will help absorb the shimmy energy until the angle has been reduced below the value where the tire skids. In addition, if the tire skids, the shimmy conditions are altered and the damping formulas no longer hold. In general, however, it has been found that if the friction damping is sufficient to prevent shimmy up to the angle at which the tire begins to skid it will prevent shimmy at all angles. It is considered advisable, however, to use a centering device to line up the wheel with the airplane so that the angle will be small at the time of ground contact.

Howard[7] has shown that the friction torque necessary to prevent shimmy in terms of the viscous damping is

$$T = (\pi/4) V \omega \theta_{max.} K \qquad (50)$$

where V = the forward velocity, ω = circular frequency of the shimmy, $\theta_{max.}$ = angle to path at which wheel touches ground, and K = viscous damping necessary to prevent shimmy at the same forward speed.

An expression is also developed for the angle, θ_0 at which the tire will begin to skid sideways. This angle is given in terms of the tire constants as

$$\theta_0 = C_2 \mu W / E_\lambda \qquad (51)$$

where μ = skidding coefficient of friction of tire and W = load on wheel.

From Eqs. (48), (49), (50), and (51), a general expression was derived for the frictional torque. Substitution of the general values of tire characteristics mentioned

earlier in this expression reduces it to the simple form of

$$T_{max.} = 0.06r\mu W \text{ ft.lb.} \tag{52}$$

where r is the tire radius in ft.

The constant, 0.06, is a maximum value, checked by test. Apparently the expression for the skidding angle leads to erroneous results in some cases, since simple substitution of the tire characteristics in the general expression for $T_{max.}$ gives constants in Eq. (52) varying from 0.02 for streamline tires to 0.06 for low-pressure and air wheel tires. In full-scale shimmy tests, however, the constant was found to have a value between 0.04 and 0.06 for a skidding coefficient of friction, μ, of 0.55. The experimental error is probably about the amount of this variation.

Returning to Fig. 19 and considering now the curve for mathematically hydraulic or velocity squared damping, it can readily be shown that this type of damping could never be used alone to eliminate shimmy. The hydraulic damping torque is given by the equation

$$T = K_h\dot{\theta}^2 \tag{53}$$

where K_h = a constant for the dampener and $\dot{\theta}$ = angular velocity of shimmy.

This is the equation of a parabola symmetric about the torque axis. Since at the origin or for zero angular velocity the slope of this parabola is zero while the slope of the required damping as shown by the viscous damping line remains constant, the hydraulic damping will always be less than necessary to prevent shimmy at low-angular velocities. As the shimmy velocity increases, the hydraulic damping torque, increasing with velocity squared, crosses the viscous damping torque line and for higher velocities supplies an excess of damping torque. Therefore, with a hydraulic dampener, the shimmy would build up to an amplitude where the excess over the required viscous torque during the high-velocity part of the cycle would absorb sufficient energy to balance the deficiency during the low-velocity part of the cycle. The hydraulic dampener would therefore limit the maximum amplitude the shimmy could maintain but would not eliminate it entirely.

Construction of Fluid Dampeners

Fluid dampeners used on airplanes to date have been of two general types: the vane, or automobile shock absorber type, and the oleo cylinder type. The Houde Engineering Corporation of Buffalo, N.Y., has kindly supplied information on the history of their development of vane-type, nose wheel shimmy dampeners and valuable engineering data on dampener characteristics and sizes.

The vane-type dampener operates by compressing oil between two rotatable and two fixed radial vanes enclosed in a metal cylinder, thus forcing the oil through orifices in a central shaft to which the movable vanes are attached. Clearances between the rotating and fixed parts are kept as small as possible, and the cylinder is kept full at all times by an oil reservoir maintained under positive pressure by a spring-loaded plunger and connected to the cylinder through check valves. An adjustable temperature-compensating valve controls the orifice sizes in the central shaft. This valve permits adjustment of the amount of damping and, once set, automatically corrects for changes in the oil viscosity with temperature. The general construction is shown schematically by the sketch of a section through the damping cylinder in Fig. 20. The angle through which the movable vane may be rotated is usually limited by clearances to not more than 60 deg. either side of the neutral position. There is also a practical limit on closing the orifice valve, since shutting the valve down too much increases the resistance at low-angular velocities to a point where steering is made difficult. Dampeners in use at present have generally been operated with the control valve about half closed, in which range they develop around 30 per cent of their maximum possible damping torque.

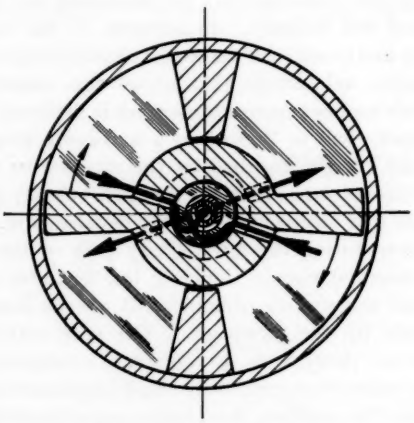

FIG. 20. Section through the cylinder of a vane-type dampener. For clockwise rotation of the movable vanes, oil flows into the center along the heavy solid line (passing through the orifice regulated by turning the innermost tube) to the central tube, down the tube and out along the heavy dashed lines.

The vane-type dampener has the advantage that it may be installed inside the shock strut piston and can even be made an integral part of the piston by using the piston wall for the dampener cylinder if desired. On this type of installation the dampener shaft extends out of the bottom of the piston and is restrained against turning by a scissors link connecting it to the shock strut cylinder. With this method the dampener case and attached vanes turn when the wheel casters while the central shaft and vanes remain fixed. If it is desired to have the dampener more accessible, it may be mounted on a bracket attached to the shock strut cylinder. A scissors link is then used to carry the castering wheel torque from the shock strut piston to a collar pivoting about the shock strut cylinder. This collar is then connected by a torque arm and push rod to a

torque arm on the dampener shaft. If it is desired to have the nose wheel caster more than the 120-deg. limit of the dampener, the torque arm on the collar can be made shorter than that on the dampener or an eccentric drive may be used at the collar to permit 360-deg. rotation of the nose wheel. With the eccentric drive the damping would become zero for the 90- and 270-deg. positions of the nose wheel, but this would have no serious effect since this position would only be used for ground handling.

On the first two installations of a vane-type nose wheel shimmy dampener the correct size was determined experimentally on three-wheeled carts that simulated the actual airplane landing gears. Later, experiments were conducted by towing nose wheel assemblies behind a truck as a one-wheel trailer. It was found that extremely small dampeners would eliminate shimmy if operated with the control valve sufficiently closed but that the resultant high-operating pressures in the chamber made steering difficult. By using larger dampeners with the orifice valve well open, operating characteristics were obtained which produced little resistance at the low-angular velocities encountered in steering, yet provided adequate damping under shimmy conditions. The minimum satisfactory dampener size is therefore not the smallest size that prevents shimmy but the smallest size that does not impede steering while preventing shimmy. It was found that for conventional nose wheels the desired result could be obtained by limiting the maximum value of the ratio between the nose wheel static load and the dampener torque per unit internal pressure. Approximately, this corresponds to making the dampener internal cylinder volume directly proportional to the nose wheel load. Successful dampeners have been designed in this manner for nose wheels with static loads ranging from 350 to 12,000 lbs. Fig. 21 shows an approximate, empirical relation derived by plotting the total internal dampener cylinder volumes against the static loads of the corresponding nose wheel assemblies for some 20 dampeners. This relationship is given primarily to permit estimates of space requirements in preliminary nose gear design work. The cylinders on which Fig. 21 is based cover a range of values of diameter to height ratio of from 1.5 to 0.75 and, although the damping is theoretically independent of this ratio, caution should be used in estimating sizes outside this range. Dampener overall dimensions are only slightly greater in diameter than the oil cylinder but are usually three to four times its length because of the packing glands, torque arm, and oil reservoir.

In the initial vane dampener development work, it was found impossible to check the damping experimentally determined with that calculated in accordance with the method of Kantrowitz[4] by use of his theoretic tire constants. The full-scale tests proved so satisfactory that no further attempt was made to apply the theoretic method. However, an independent check by

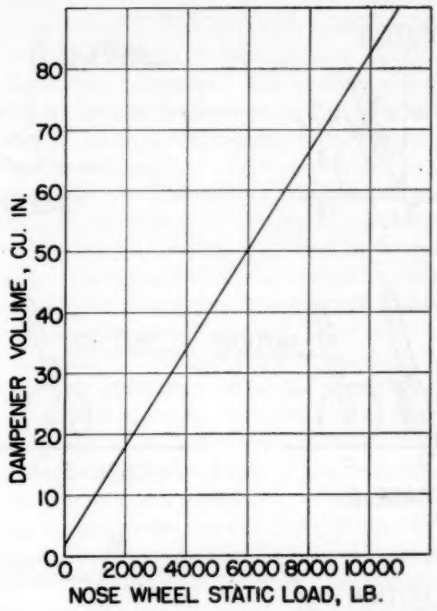

FIG. 21. Empirical relation between internal cylinder volume of vane-type shimmy dampeners and static nose wheel load.

the authors, using the extrapolated tire constants derived by Howard[7] from full-scale tests, gave good agreement on one installation. The calculated damping was slightly less than that of the actual dampener with the control valve half closed. Data was not available for direct checking of other installations, but Wylie[3] shows good agreement in one case and Howard has shown fair agreement for the theoretic method when applied to dry friction damping. Since the determination of the dry friction damping requires assumptions concerning the skidding angle not necessary for finding the fluid damping, it is logical to expect greater accuracy with fluid dampeners.

Dampeners using a piston in an oil-filled cylinder have been used on several nose wheels. The by-pass valve may be located in the piston or in a pipe connected to each end of the cylinders. The installation is made on a bracket on the shock strut cylinder in the same manner as the bracket installation of the vane-type dampener. No information is available as to sizes or damping characteristics of actual piston dampeners, but it should be possible to approximate the damping properties by hydraulic theory.

By omitting the by-pass valves and connecting a rudder-controlled, oil pressure source to opposite sides of the movable vanes or piston, it is possible to steer the nose wheel with either the vane- or piston-type dampener. The dampener thus can be made to perform the dual functions of a steering and an antishimmy device.

Several dampener installations have shown the importance of rigidity in the linkage between the wheel and the dampener. Any play will permit small oscilla-

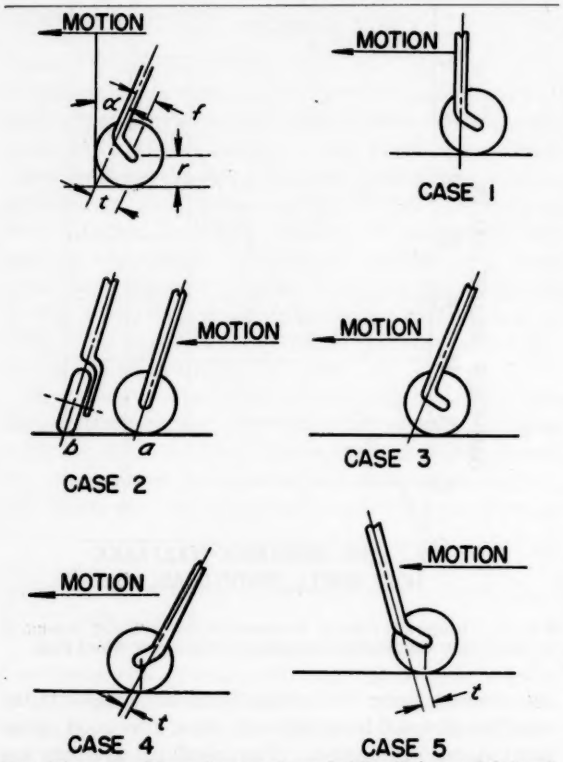

FIGS. 22 to 27. Dimensions as shown in Fig. 22 (upper left-hand corner) are positive.

tions before the dampener begins to take effect, and these oscillations may cause fatigue failures, loosening of joints, and similar difficulties. It is recommended that the scissors links have forked joints and be of torsionally resistant sections to reduce deflections. The damping torque should be considered in the design of the nose wheel strut in addition to the usual loads, especially in drift landing conditions where the wheel must caster quickly upon striking the ground.

GROUND HANDLING AND MANEUVERABILITY

General

The ground-handling and maneuverability characteristics of a tricycle landing gear are largely controlled by the nose wheel properties of trail, caster angle and castering friction, and the general gear dimensions of main wheel tread and distance aft of the airplane c.g. The effects of tread and rear wheel location were discussed under "Directional Stability and Ease of Steering" (Part 1). The factors relating specifically to the nose wheel will be considered here.

Effect of Caster Angle and Wheel Offset

With various arrangements of caster angle and trail, a castering wheel will tend to come to rest at different angles of yaw at zero forward velocity. The trail, of course, must always be positive—that is, the tire load point must be behind the caster axis in the plane of the wheel. This condition may be produced by several possible combinations of caster angle and wheel offset. These combinations are: (1) zero caster angle and positive wheel offset, (2) positive caster angle and no offset, (3) positive caster angle and positive wheel offset, (4) positive caster angle and small negative wheel offsets, and (5) small negative caster angle and considerable positive wheel offset. Mathematically, the trail may be given for the centered wheel position as shown in Fig. 22 by

$$t = f + r \sin \alpha > 0 \qquad (54)$$

where t = the trail, r = the wheel rolling radius, f = the wheel offset, and α = the caster angle.

The first combination shown in Fig. 23 is stable at any angle of yaw at zero forward velocity, and the trail remains constant throughout 360 deg. of castering. This type of installation is ideal for ground handling, since at low forward speeds the wheel does not seek a particular position but follows the caster axis. The trail, remaining constant with angle of yaw, provides large moments tending to turn the wheel to a new course even for sudden changes of course of large magnitude.

The second combination (Fig. 24) tends to turn 90 deg. from the centered position when at rest as shown by "b" since in this position the wheel center is lower than in position "a." In position "b," the effective trail tending to make the wheel follow the caster axis has become zero. Therefore, in use, this combination must be restricted against castering through angles greater than about 60 deg., otherwise the wheel will turn crosswise and prevent forward motion of the airplane. This arrangement is not good for low-speed taxiing and ground handling since the wheel tends always to caster around against the stops. The initial resistance is usually high, particularly in starting up, and it is frequently necessary to start moving in the direction the wheel is pointed and change to a straight course after the wheel speed becomes sufficient for the friction castering torque to steer the wheel.

The third combination, positive caster angle and positive wheel offset as shown in Fig. 25, will seek a position when stopped 180 deg. from the centered position. Since stops are usually used to limit the maximum angle of yaw to about 60 deg., the wheel will come to rest against the stops. For a 90-deg. yaw the effective trail is reduced from $(f + r \sin \alpha)$ to f, the wheel offset. This is comparable to Case 2 where the trail disappeared entirely, since it was all produced by caster angle. In Case 3, which may be considered a combination of Case 1 and Case 2, the trail due to wheel offset remains constant but that due to caster angle changes with angle of yaw. This arrangement will have appreciably more moment tending to straighten the wheel out when motion starts but will still be awkward for pushing or towing.

The fourth combination (Fig. 26) is the case used on the front wheels of bicycles but, so far as is known, never used on airplanes. It can be obtained by revolving the wheel in Case 3 through an angle of yaw of 180 deg., providing the offset is not too large. Case 4 inherently tends to remain in the centered position when at rest just as Case 3 tends to turn 180 deg. from it. Case 4 is stable in motion, however, only if the positive component of the trail due to caster angle is greater than the negative part due to the negative offset. It has been shown in Cases 2 and 3 that the trail due to caster angle decreases as the wheel is yawed, becoming zero for a yaw angle of 90 deg. Therefore, in Case 4 there is an intermediate angle of yaw between 0 and 90 deg., at which the trail becomes negative and the wheel directionally unstable. For this reason this type of castering unit is satisfactory only for small angles of yaw and, therefore, has not been used on aircraft.

The fifth combination (Fig. 27), negative caster angle and a large enough wheel offset to make the trail positive, is frequently used on tail wheels. This combination tends to assume the centered position when at rest. Inasmuch as the trail is the sum of a negative component from the negative caster angle and a positive component from the offset, the effective trail will increase with angle of yaw, the reason being that the negative component due to caster angle becomes smaller as the wheel is yawed. The tendency of the wheel to track (or follow the caster axis), therefore, increases as the wheel is yawed. This type of installation has good ground-handling characteristics, since the wheel is centered and offers a minimum resistance to forward motion at the instant of starting. The start may also be made straight ahead without waiting for the wheel to straighten out as is necessary in Cases 2 and 3. The tendency of the wheel to center, however, is not sufficient to interfere appreciably when the airplane is being pushed or towed. In most cases this installation does present structural complications that have prevented its use for nose wheels.

Effect of Friction in Castering Bearings and Dampener

Friction in the castering system obviously tend to make ground handling and steering difficult. The amount of friction in any particular installation is determined principally by the design of the castering bearings, the bending moment and thrust on the bearings, and the resistance of the shimmy damping system. Castering, in most nose wheels, is made possible by letting the shock strut piston rotate in the cylinder. In such cases, it is also probable that the friction varies with the shock strut extension. At extremely low speeds the friction between the tire and the ground adds to the other frictions to further impede steering.

Little information is available on the magnitude of these frictions found in service or on the maximum total friction that will still give satisfactory ground-handling characteristics. The indication is that the dampener resistance is of much greater significance than the bearing friction. The dampener resistance depends on the kind and amount of damping used and the characteristics of the dampener. The amount of damping necessary is partially determined by the trail, while the trail, in turn, controls the steering moments that must overcome the friction.

Considerable experimentation has been done with solid friction dampeners, and it has been quite thoroughly proved by Howard[7] that solid friction dampeners make steering unsatisfactory except on very light airplanes. Fluid dampeners, consequently, have usually been used to prevent shimmy. The resistance of a fluid dampener at the low-angular velocities used in steering is largely determined by the pressure per unit torque at which it operates. The smaller the dampener, the higher the fluid pressure must be for a given torque. A large dampener, operating at a low pressure, will, therefore, produce less resistance to steering than a small, high-pressure one capable of supplying the same amount of damping. Because of space and weight limitations, it is desirable to make the dampener as small as possible and still retain satisfactory steering characteristics. Mention was made previously that most vane-type fluid dampeners are operated with the control valve in the position where only about 30 per cent of the maximum damping torque is developed. This percentage torque was found to be the maximum for satisfactory steering in two installations that were used as a yardstick for other installations. The yardstick installations had particularly small trails and, consequently, small steering moments. This was particularly true at large angles of wheel yaw, since the trail was entirely due to caster angle and, accordingly, diminished when the wheel was yawed as in Fig. 24. It is probable, therefore, that a nose wheel with a larger trail would steer properly under much more severe conditions, especially if the trail were the result of wheel offset so that it did not decrease with angle of yaw. Increase in trail slightly raises the amount of damping necessary to prevent shimmy, but it may be that for moderate trails the wheel steering moment will be improved sufficiently to make it possible to obtain the increased damping from a considerably smaller, but more efficiently operated, dampener. Thus, a moderate increase in trail, though requiring more damping, might make possible the use of a smaller dampener.

Values of trail recommended by various authors vary from 16 to 50 per cent of the tire radius. Positive caster angles of from 8 to 20 deg. are also usually advocated. Experience indicates that a trail of from 25 to 50 per cent of the radius is generally most satisfactory. This range of trail was found by Wernitz[8] to be used on most designs in service.

Ease of Installation and Construction

Throughout the preceding discussion on nose wheel design, the problem has been approached only from the

standpoint of obtaining satisfactory performance from the landing gear without reference to possible installation and construction difficulties. A few problems that may involve compromises with the performance criteria will be considered here.

On most airplanes, especially single-engined tractors, it is usually structurally desirable to have the nose wheel strut slope forward from the airplane. This arrangement permits a reduction in the length of structure subjected to the nose wheel loads and also reduces the bending moments on the strut due to drag loads on the wheel. Since the strut is usually the castering axis, this arrangement produces a positive caster angle that requires more damping to prevent shimmy and interferes somewhat with ground-handling characteristics. The arrangement of a small negative caster angle that requires minimum damping and centers the wheel when at rest would require the strut to interfere with the propeller in order to keep the same wheel base. Probably the best that can be used with a single nose wheel strut is a caster angle of zero. These considerations may be altered, of course, if an unconventional nose wheel support is used.

The bending moment on a single-strut nose wheel support is also increased by wheel offset, which thus places the vertical wheel load behind the strut axis. In addition, wheel offset may complicate the retracting problem on wheels that are turned crosswise when retracted, since it will ordinarily result in the wheel being off the airplane centerline in the retracted position. It is possible in some cases to eliminate this difficulty by revolving the wheel during retraction about an axis through the wheel centerline and the top of the strut rather than the strut axis. This would involve some complication of the system, however, and is naturally to be avoided when retracting space permits.

Steering Devices, Stops, Locks

It is desirable in many cases to equip nose wheels with an irreversible steering device connected to the rudder pedals for use in low-speed taxiing. This device must be arranged to be disconnected by the pilot at will and should steer the nose wheel through an angle sufficient to enable the airplane to turn about one main wheel as a pivot. Other airplanes sometimes use a centering lock or catch, together with stops, limiting the throw of the nose wheel to the angle necessary to pivot about one main wheel.

Stops, used to limit the wheel throw, should be designed to take appreciable loads, since their failure will usually result in damage to the dampener from exceeding its allowable angular range. This damage may not be detected and thus may result in violent shimmy and strut failure on the next flight. A suggested design criterion for these stops is the torque resulting from a force perpendicular to the wheel at the load point sufficient to cause the wheel to skid sideways under its normal static load. This torque may be considered approximately equal to the static nose wheel load times the trail. The same criterion would also apply to steering devices and locks.

Comparison of Design Criteria with Characteristics of Existing Airplanes

General

As an approximate check of the validity of the criteria previously developed, the characteristics of three successful tricycle landing gear airplanes were determined and compared with the criteria. The characteristics determined were the resistance to turning over and the longitudinal stability when taxiing on the two rear wheels. The effective weight acting on the nose wheel was also determined for two of the airplanes and compared with the nose wheel static load. Lack of information on other airplanes prevented the determination of their characteristics, but it is hoped that data can be obtained in the future to make possible further comparison of the criteria with design practice.

Criteria for Stability When Taxiing on the Rear Wheels

The longitudinal stability of the three airplanes when taxiing on the rear wheels was determined by the methods developed earlier using Figs. 5 and 6 (Part 1).

The results obtained from this procedure indicate that all three airplanes definitely satisfy the stability criteria. The actual rear wheel distance aft of the aerodynamic center was from 5 to 30 per cent less than the maximum permissible distance for stability in the horizontal position. Thus, with increase in angle of attack these airplanes would become even more stable due to the decrease in p. The evidence, although not complete, indicates that the stability criterion should be adhered to, at least until some evidence to the contrary is produced.

Criteria for Stability Against Overturning

The minimum satisfactory tread in per cent of the wheel base was determined by the use of Fig. 9 (Part 1). The three airplanes were found to exceed the criterion by 2, 9, and 15 per cent, respectively.

Dimensions of other airplanes were not directly available but were approximated by scaling small three-view drawings. It was found that all except one were stable for coefficients of friction up to at least 0.8. The coefficient used in developing the criteria was 0.85. The one exception would resist overturning for frictional coefficients less than 0.62. This airplane was converted to a tricycle gear amphibian as an afterthought, having originally been designed as a flying boat. As a consequence, practical difficulties probably prevented providing a more adequate tread and made it necessary to use a lesser degree of stability, with a corresponding reduction in the ability to land cross wind. In general, it was found that the larger and

faster airplanes had a slightly greater degree of stability than the smaller and lighter models.

It is apparent that adherence to the criteria for overturning will produce an airplane with satisfactory characteristics in this respect, since there is no record of any difficulty of this type with any of the airplanes complying with it. There is some indication that a small reduction in the coefficient of friction may be made without sacrificing any of the desirable features of the landing gear. Further reductions in stability will probably seriously limit the angle of drift at which the airplane may be safely landed.

Comparison of Nose Wheel Loads in Three-Wheel and Nose First Landings

The percentage of vertical kinetic energy absorbed by the nose wheel in nose first and three-wheel landings was determined by Eqs. (1) and (9) for two of the airplanes. Lack of the pitching radius of gyration prevented the determination for the third airplane.

For one, it was found that, in a three-wheel landing, 11.3 per cent of the kinetic energy is absorbed by the nose wheel compared to 39.4 per cent in the nose first landing. For the other, the percentages are 18.5 per cent, maximum, in a three-wheel landing and 26.8 per cent, maximum, in a nose first landing. Thus, for the same sinking speed in both landing conditions, the nose wheel of the former is subjected to a load in a nose first landing three and one-half times that in a three-wheel landing, while the nose wheel of the latter would get only one and one-half times the three-wheel landing load. As these airplanes are multiengined designs of about the same weight and size yet differ widely in the ratio of nose wheel loads in the two landing conditions, the only conclusion that can be drawn is that the nose wheel load is dependent on the type, as well as the size, of the airplane.

Based on the above percentage, the tire of the first airplane is 62 per cent overloaded for a nose first landing or, what amounts to the same thing, for fast taxiing on rough ground. It is reported that some difficulty has been experienced with this installation, and it is believed that more severe design conditions than the usual three-wheel landing are justified. It is felt, therefore, that consideration should be given to this landing condition in any new designs and that landing tests should be made to determine actual sinking speeds and accelerations in nose first landings. In the meantime, conservative assumptions of the sinking speed should be used on all nose wheel designs.

Conclusions

By analysis of the theories and data presented, the following conclusions may be obtained.

Effects of Wheel Base

1. Increase in the distance of the nose wheel forward of the c.g. rapidly reduces the critical design loads on the nose wheel, decreases the probability of pitching oscillations, and increases the resistance of the airplane to turning over.

2. The distance of the rear wheels aft of the c.g. must be sufficient so that the c.g. will be forward of the rear wheels with the airplane in the tail-down attitude. At the same time, the distance aft of the wing aerodynamic center should not exceed the maximum value at which the airplane will be longitudinally stable when taxiing on only the rear wheels at take-off speeds.

3. An increase in the distance of the rear wheels aft of the c.g. also results in increased directional stability, a small reduction in the resistance to overturning, and a reduced likelihood of pitching oscillations during taxiing on all three wheels.

Effects of Tread

1. The tread should be sufficient so that in a landing with side drift the wheels will skid sideways and not overturn the airplane.

2. The larger the tread, the more maneuverable the airplane will be while taxiing.

3. Satisfactory ratios between the values of wheel base and tread are best obtained by careful application of the criteria and cannot be arbitrarily defined.

Effects of Caster Angle

1. Positive caster angle increases the tendency to shimmy and requires additional damping.

2. Positive caster angle causes the nose wheel to turn crosswise when stopped, increasing the difficulties of ground handling and steering at low speeds.

3. Positive caster angle more nearly aligns the nose wheel strut with the resultant forces it must resist and thus reduces the bending moments.

4. Positive caster angle makes it possible to use a shorter nose structure on the airplane for the same wheel base.

5. Negative caster angles up to about 8 deg. decrease the tendency to shimmy.

6. Negative caster angles make the nose wheel center when stopped.

7. For zero caster angle the nose wheel neither centers nor turns crosswise when stopped but remains pointed in the direction in which it was last rolling.

8. From the standpoint of handling characteristics and damping requirements, a zero caster angle is preferable. Structural requirements may, however, necessitate the use of a positive caster angle.

Effects of Trail

1. The trail must be positive at all times, at all possible angles of yaw of the nose wheel, and at all encounters of the nose wheel with obstructions.

2. Increase in trail increases the tendency to shimmy and requires additional damping.

3. Increase in trail improves the steering and ground-handling characteristics.

4. It is possible that an increase in trail may permit reducing the dampener size, since the improvement in steering torque available may compensate for the additional resistance of a smaller dampener absorbing a larger damping torque.

Effects of Tire

1. All rubber-tired castering wheels will shimmy unless equipped with a damping device or other means of shimmy prevention.

2. The amount of damping necessary to prevent shimmy can be estimated if certain characteristics of the tire and its installation are known.

3. Streamline tires require the most viscous damping; airwheel tires, the least; low-pressure tires are intermediate. The order is reversed when solid friction damping is used, although in this case little difference between tires can be detected.

Effects of Moment of Inertia of Castering Parts

1. The viscous damping necessary increases with the moment of inertia of the castering parts.

2. The solid friction damping required is independent of the moment of inertia of the castering parts.

Effects of Type of Damping Used to Prevent Shimmy

1. Solid friction damping makes steering and ground handling too difficult to be satisfactory except on very small airplanes.

2. Fluid dampener size is apparently controlled not by the smallest dampener that can prevent shimmy but by the smallest dampener capable of providing the necessary damping, together with a small enough resistance at low-angular velocities to produce satisfactory steering characteristics.

3. The amount of any particular type or combination of types of damping necessary to prevent shimmy in a particular installation may be approximated mathematically.

REFERENCES

[1] Stalker, E. A., *Principles of Flight*, The Ronald Press Company, New York, 1931.

[2] Wetmore, J. W., *The Rolling Friction of Several Airplane Wheels and Tires*, N.A.C.A. T.R. No. 583, Washington, D.C., 1937.

[3] Wylie, Jean, *Dynamic Problems of the Tricycle Alighting Gear*, Journal of the Aeronautical Sciences, Vol. 7, No. 2, pp. 56–67, December, 1939.

[4] Kantrowitz, A., *Stability of Castering Wheels for Aircraft Landing Gears*, N.A.C.A. T.R. No. 686, Washington, D.C., 1940.

[5] Taylor, J. Lockwood, *Oscillation of Castering Wheels*, Aircraft Engineering, Vol. 13, No. 143, p. 13, January, 1941.

[6] Warner, E. R., *The Double Spindle Wheel Castering System for Airplane Nose Wheels*, Cleveland Pneumatic Tool Company, Cleveland, O.

[7] Howard, Walter B., *A Full Scale Investigation of the Effect of Several Factors on the Shimmy of Castering Wheels*, N.A.C.A. T.N. No. 760, Washington, D.C., 1940.

[8] Wernitz, W., *Tricycle Undercarriage Development*, Aircraft Engineering, Vol. 13, No. 143, pp. 6–12, January, 1941; Translated from Luftwissen, Vol. 7, No. 3, March, 1941.

[9] Schilling, R., and Fuchs, H. O., *Modern Passenger-Car Ride Characteristics*, Journal of Applied Mechanics, Vol. 8, No. 2, pp. A-59–A-66, June, 1941.

Erratum

In the article "Dynamic Balancing as Applied to Transport Aircraft Propellers," by Dixon Speas and John C. Luttrell, in the July, 1942, issue of the JOURNAL, the caption of Fig. 2 should be corrected so that the fifth sentence reads: "Slope of inclined lines is 0.04." Also, inking of reproduction (B) in the same figure makes 2.6 appear to be 2.3.

Rotor Bending Moments in Plane of Flapping

ALEXANDER KLEMIN,* W. C. WALLING,† AND WAYNE WIESNER‡

New York University and Kellett Autogiro Corporation

SUMMARY

The present paper, a problem in autogiro rotor stress analysis, can be outlined as follows:

1. Calculation of the characteristics of a typical autogiro employed for illustrative purposes.
2. Derivation of formulas for bending moments in the plane of flapping taking into account the effects of the weight of the blade, centrifugal force, inertia forces in flapping and aerodynamic thrust.
3. Examination of the effect of the azimuth angle Ψ on bending moments at a given point on the blade.
4. Effect of variations in μ, the tip speed ratio, on the bending moment at a given point on the blade.
5. Examination of the effect of the ratio r/R on bending moments.
6. Formulas for the centrifugal relief of bending moments.
7. Comparison of bending moments obtained by the above methods with the bending moments obtained by the use of empirical formulas available hitherto.

Certain simplifications have been employed. These are:

(a) Only the first harmonic of the flapping motion is considered.
(b) Terms of a higher order than μ^2 are neglected.
(c) The flow through the rotor disk is considered uniform.
(d) Mass distribution along the span of the blade is uniform.
(e) The product EI is uniform along the span of the blade.
(f) Stalling effects that may occur at portions of the blade are neglected.
(g) Periodic twisting of the blade is not taken into account.

The underlying aerodynamic theory is well known to those interested in the autogiro and no presentation of such theory is made in the present paper.

SYMBOLS USED

R = tip radius of the blade in feet
r = radius at an intermediate point in feet
ω = angular velocity in radians per sec.
m = line density of a blade in slugs per ft.
Ψ = angle in radians measured from the rearmost position of a blade
Ψ_1 = angle in radians defining the lowest position of the blade with reference to the plane of rotation
β = $\beta_0 - \beta_1 \cos(\Psi - \Psi_1) = a_0 - a_1 \cos\Psi - b_1 \sin\Psi$ = alternative expressions for coning or flapping angle
i = angle of attack of the plane of rotation
μ = $V \cos i/\omega R$ = nondimensional tip speed ratio
θ = angle of blade setting from line of no lift to plane of rotation in radians
ϕ = induced angle = U_y/U_x in radians
α = $\theta + \phi$ = angle of attack of a blade element in radians
a_∞ = lift slope coefficient referred to radians = 6
u = flow through disk of rotation
U_x = velocity at right angles to an element of the span of the blade in the plane of rotation, in ft. per sec. = $r\omega + \mu R\omega \sin\Psi$
U_y = resultant velocity at a blade element at right angles to the plane of rotation = $xR\omega + e_0 + e_1 \cos\Psi + f_1 \sin\Psi + e_2 \cos 2\Psi + f_2 \sin 2\Psi$

Where $x = u/\omega R$ $\quad e_0 = a_1\mu R\omega/2$ $\quad e_1 = b_1 r\omega - a_0\mu R\omega$
$f_1 = -ra_1\omega$ $\quad e_2 = a_1\mu R\omega/2$ $\quad f_2 = b_1\mu R\omega/2$

I_H = moment of inertia of a blade about the horizontal hinge in slugs sq.ft. = $mR^3/3$
γ = nondimensional constant = $3c\rho R^4/I_H$
a_0 = average flapping angle in radians
a_1 = longitudinal flapping constant in radians
b_1 = lateral flapping constant in radians
δ = mean profile drag coefficient
T_1 = expression for thrust of a single blade in lbs.
A_r = $\int_R^r \int_R^r dr$, $B_r = \int_R^r \int_R^r r\,dr$, $C_r = \int_R^r \int_R^r r^2\,dr$
M = bending moment for a flexible blade at any point of a blade, positive when concavity is on the upper surface in ft.lbs.
M_{RG} = bending moment for a rigid blade
M_w = bending moment due to the weight of the blade at any point of the blade
M_{CF} = bending moment due to centrifugal force at any point of the blade
M_I = bending moment due to inertia forces in flapping at any point of the blade
M_T = moment due to aerodynamic thrust at any point of the blade

CALCULATION OF THE CHARACTERISTICS OF A TYPICAL AUTOGIRO

Characteristics of a Typical Autogiro

KD-1B Autogiro with rectangular blades (Kellett Air Mail Giro).

R	= 20 ft.	δ	= 0.006 (0.012 in calculation)
S	= 1,256 sq.ft.	E	= 29,000,000 lbs. per sq.in.
W	= 2,275 lbs.	I_H	= 200 lbs. ft. sec.^{2}
BcR	= 60 sq.ft.	W_1	= 48.3 lbs.
σ	= 60/1,256 = 0.0478	m	= 0.075 lb. sec.^{2} sq.ft.
w	= 1.81 lbs. per sq. ft.	I_S	= 0.135 in.^{4}
θ	= 3 deg. = 0.0524	γ	= $3c\rho R^4/I_H = 5.71$
C	= 1 ft.		

Formulas for Parameters

The aerodynamic characteristics of the rotor are calculated with the aid of the following formulas:

The nondimensional constant relating the aerodynamic forces and moments to the moment of inertia of a flapping blade:

$$\gamma = 3c\rho R^4/I_H \qquad (1)$$

Presented at the Rotating Wing Aircraft Session, Tenth Annual Meeting, I.Ae.S., New York, January 29, 1942.

* Guggenheim Research Professor of Aeronautics.
† Research Assistant.
‡ Aerodynamicist.

The coefficient of disk flow, $x = u/\omega R_1$:

$$\frac{\delta}{12}(1 + \mu^2) = x\left(x + \frac{2}{3}\theta\right) + \frac{1}{18}\gamma^2\mu^2\left(\frac{x}{3} + \frac{\theta}{4}\right)^2 \quad (2)$$

where μ is assigned a value arbitrarily, which is kept throughout a series of calculations.

The coefficient of thrust:

$$T_c = \sigma\left[\theta\left(1 + \frac{3\mu^2}{2}\right) + \frac{3x}{2}\right] \quad (3)$$

Angle of attack of the rotor i:

$$\tan i = (x + {}^1/_2T_c)/\sqrt{\mu^2 + x^2} \quad (4)$$

A tip-speed ratio:

$$\lambda = \mu/\cos i \quad (5)$$

The tip speed in ft. per sec.:

$$\omega R = \sqrt{w/T_c\rho} \quad (6)$$

Forward speed, in ft. per sec.:

$$V = \lambda\omega R \quad (7)$$

The average flapping angle in radians:

$$a_0 = \gamma[(x/3) + (\theta/4)(1 + \mu^2)] - C \quad (8)$$

where

$$C = \frac{\int_0^R mgr\,dr}{I_H\omega^2} = \frac{mgR^2/2}{m\omega^2R^3/3}$$

The longitudinal flapping constant in radians:

$$a_1 = \mu[(8\theta/3) + 2x] \quad (9)$$

The lateral flapping constant in radians:

$$b_1 = {}^4/_3a_0\mu \quad (10)$$

Alternative Values of a_1 and b_1 (a_1' and b_1')

There are possible alternative relationships:

$$a_1' = {}^3/_4\mu^2\theta \quad (11)$$

$$b_1' = 3a_0\mu/4 \quad (12)$$

which are employed when dealing with second harmonic terms in the expression for the thrust moment. The last two equations appear contradictory with Eqs. (9) and (10) but, since they involve neglect of terms in μ^3, the contradiction is only apparent.

It is well known that when the flapping is represented by a constant and a first harmonic the moment of the thrust at the flapping hinge is independent of the azimuth angle Ψ. It is by making use of this fact and equating the periodic terms in the expression for thrust moment to zero that Eqs. (9), (10), (11) and (12) are derived. When, however, terms of higher order than μ^2 are neglected, there appear to be available four equations for the evaluation of two unknowns, namely, a_1 and b_1. Equation (9) is obtained by equating to zero, at $r = 0$, the periodic term in cos Ψ and Eq. (10) by equating to zero, at $r = 0$, the periodic term in sin Ψ. Therefore it is entirely logical in evaluating periodic terms in cos Ψ and sin Ψ to use the values of a_1 and b_1 derived from Eqs. (9) and (10), respectively. But when dealing with expressions in cos 2Ψ, it will be empirically more accurate to use Eq. (11), and with expressions in sin 2Ψ to use Eq. (12).

Calculation of Rotor Characteristics

With the above data and the aid of the above equations, the aerodynamic characteristics of the rotor have been calculated in Table 1 for $\mu = 0.3$, 0.4 and 0.5. In the calculations the further approximation has been made that cos $i = 1$. The table indicates that ω drops off slightly as μ increases, which is contrary to practical experience. The discrepancy is not large and does not invalidate the general treatment. It does indicate, however, that to secure a better approximation to the value of ω it is necessary to take orders greater than μ^2 into account.

TABLE 1

Aerodynamic Characteristics of the Rotor for Various Values of μ, with $\gamma = 5.71$, $\theta = 3° = 0.0524$, $\sigma = 0.0478$, $R = 20$ ft.

Value of μ	0.3	0.4	0.5
$x = u/\omega R$	0.0190	0.0193	0.0196
T_c	0.00420	0.00450	0.00485
ωR	426	412	396
ω	21.3	20.6	19.8
$V\ (= \mu\omega R)$	128	165	197
a_0	0.1126	0.1181	0.1247
C	0.005	0.005	0.005
a_1	0.0535	0.0714	0.0895
b_1	0.0450	0.0630	0.0831
a_1'	0.0118	0.0157	0.0197
b_1'	0.0253	0.0355	0.0467
R.p.m.	204	197	190
V (m.p.h.)	87	113	134

DERIVATION OF FORMULAS FOR BENDING MOMENTS IN THE PLANE OF FLAPPING

The formulas are derived in the following order: moment due to (1) weight of the blade, (2) centrifugal force, (3) inertia force in flapping, and (4) aerodynamic thrust. The sign of the moment at a point on the span of the blade is taken as positive when the concavity is on the upper surface of the blade. The distance of the flapping hinge from the center of rotation is neglected. In dealing with the well-known expression of applied mechanics, $M = \int\int w\,dx\,dx$, it is convenient to introduce auxiliary functions for the double integration as:

$$\int_R^r\int_R^r dr\,dr = [(r^2/2) + (R^2/2) - Rr] = A_r \quad (13)$$

$$\int_R^r\int_R^r r\,dr\,dr = [(r^3/6) + (R^3/3) - (R^2r/2)] = B_r \quad (14)$$

$$\int_R^r\int_R^r r^4\,dr\,dr = [(r^4/12) + (R^4/4) - (R^3r/3)] = C_r \quad (15)$$

Expression for Moment Due to Weight of the Blade

The moment at any point, r, is given by

$$M_w = \int_R^r\int_R^r -mg\,dr\,dr = -mg\,[R^2/2 + r^2/2 - Rr] = -mgA_r \quad (16)$$

Expression for Moment Due to Centrifugal Force

The force in pounds per unit length due to the centrifugal force is $m\omega^2 r$ and the component of the centrifugal force at right angles to the blade and, hence, producing a bending moment is $-m\omega^2 r \sin \beta = -m\omega^2 r\beta$ approximately. Hence, the bending moment due to centrifugal force (for a rigid blade) is given by

$$M_{CF} = \int_R^r \int_R^r - m\omega^2 r\beta \, dr \, dr = -m\omega^2 \beta B_r \quad (17)$$

The moment due to centrifugal force can be submitted into a steady part, a part containing cos Ψ, and a part containing sin Ψ by inserting for β the expression $a_0 - a_1 \cos \Psi - b_1 \sin \Psi_1$ so that

$$\begin{aligned} &\text{Steady part of } M_{CF} = -m\omega^2 a_0 B_r \\ &\text{Part of } M_{CF} \text{ in cos } \Psi = m\omega^2 a_1 B_r \cos \Psi \\ &\text{Part of } M_{CF} \text{ in sin } \Psi = m\omega^2 b_1 B_r \sin \Psi \end{aligned} \quad (18)$$

Expression for Moment Due to Inertia Forces in Flapping

The inertia force per unit length is $-m\ddot{\beta}r$, the sign being negative since the load is downward when there is positive angular acceleration. Hence, the bending moment due to the inertia forces in flapping is

$$M_I = \int_R^r \int_R^r - m\ddot{\beta} r \, dr \, dr = -m\ddot{\beta} B_r \quad (19)$$

Since

$$\begin{aligned} \beta &= a_0 - a_1 \cos \Psi - b_1 \sin \Psi \\ \dot{\beta} &= a_1 \sin \Psi\omega - b_1 \cos \Psi\omega \\ \ddot{\beta} &= a_1 \cos \Psi\omega^2 + b_1 \sin \Psi\omega^2 \end{aligned}$$

Inserting this expression for $\ddot{\beta}$ in Eq. (4),

$$\begin{aligned} &\text{Steady part of } M_I = 0 \\ &\text{Part of } M_I \text{ in cos } \Psi = -m\omega^2 a_1 B_r \cos \Psi \\ &\text{Part of } M_I \text{ in sin } \Psi = -m\omega^2 b_1 B_r \sin \Psi \end{aligned} \quad (20)$$

Expression for Moment Due to Aerodynamic Thrust

If dT_1 is the value of the thrust for a blade element, then the moment due to thrust may be written as $\int_R^r \int_R^r dT_1 \, dT_1$. With the assumptions and terminology previously given, it can be readily shown that

$$\begin{aligned} dT_1 = 3c\rho[&\theta(r^2\omega^2 + \mu^2 R^2 \omega^2 \sin^2 \Psi + 2r R\mu\omega^2 \sin \Psi) + \\ &(r\omega + \mu R\omega \sin \Psi)(xR\omega + e_0 + e_1 \cos \Psi + \\ &f_1 \sin \Psi + e_2 \cos 2\Psi + f_2 \sin 2\Psi)] \, dr \end{aligned} \quad (21)$$

On the hypothesis that terms of an order higher than μ^2 may be neglected, it is possible to eliminate some of these terms.

$e_0 = a_1 \mu R\omega/2$, has order of magnitude μ^2
$e_1 = b_1 r\omega - a_0 \mu R\omega$, has order of magnitude μ^1
$f_1 = -r a_1 \omega$, has order of magnitude μ^1
$e_2 = a_1 \mu R\omega/2$, has order of magnitude μ^2
$f_2 = b_1 \mu R\omega/2$, has order of magnitude μ^2

The terms that may be neglected are therefore represented by the expression $(\mu R\omega \sin \Psi)(e_0 + e_2 \cos 2\Psi + f_2 \sin^2 \Psi)$, and for stress analysis purposes:

$$\begin{aligned} dT_1 = 3c\rho[&\theta(r^2\omega^2 + \mu^2 R^2 \omega^2 \sin^2 \Psi + 2r R\mu\omega^2 \sin \Psi) + \\ &r\omega(xR\omega + e_0 + e_1 \cos \Psi + f_1 \sin \Psi + e_2 \cos 2\Psi + \\ &f_2 \sin 2\Psi) + \mu R\omega \sin \Psi (xR\omega + e_1 \cos \Psi + f_1 \sin \Psi)] \, dr \end{aligned} \quad (22)$$

To express results in terms of constants cos Ψ, sin Ψ, cos 2Ψ, sin 2Ψ: $\cos^2 \Psi = (1 + \cos 2\Psi)/2$; $\sin^2 \Psi = (1 - \cos 2\Psi)/2$; $\sin \Psi \cos \Psi = \sin 2\Psi/2$. Substituting these trigonometric relationships in Eq. (10),

$$\begin{aligned} dT_1 = 3c\rho\Bigg[&\theta\Bigg(r^2\omega^2 + \frac{\mu^2 R^2 \omega^2}{2} - \frac{\mu^2 R^2 \omega^2 \cos 2\Psi}{2} + \\ &2r R\mu\omega^2 \sin \Psi\Bigg) + r\omega(xR\omega + e_0 + e_1 \cos \Psi + f_1 \sin \Psi + \\ &e_2 \cos 2\Psi + f_2 \sin 2\Psi) + \mu R\omega\Bigg(xR\omega \sin \Psi + \\ &\frac{e_1 \sin 2\Psi}{2} + \frac{f_1}{2} - \frac{f_1 \cos 2\Psi}{2}\Bigg)\Bigg] dr \end{aligned} \quad (23)$$

The expression for the moment due to aerodynamic thrust then becomes:

$$\begin{aligned} M_T = \int_R^r \int_R^r 3c\rho\Bigg[&\theta\Bigg(r^2\omega^2 + \frac{\mu^2 R^2 \omega^2}{2} - \frac{\mu^2 R^2 \omega^2 \cos 2\Psi}{2} + \\ &2r R\mu\omega^2 \sin \Psi\Bigg) + r\omega(xR\omega + e_0 + e_1 \cos \Psi + f_1 \sin \Psi + \\ &e_2 \cos 2\Psi + f_2 \sin 2\Psi) + \mu R\omega\Bigg(xR\omega \sin \Psi + \\ &\frac{e_1 \sin 2\Psi}{2} + \frac{f_1}{2} - \frac{f_1 \cos 2\Psi}{2}\Bigg)\Bigg] dr \, dr \end{aligned} \quad (24)$$

It is convenient to subdivide M_T into parts—namely, (1) steady part, (2) part in cos Ψ, (3) part in sin Ψ, (4) part in cos 2Ψ, (5) part in sin 2Ψ—and to integrate each part separately.

The steady part:

$$M_{T_s} = \int_R^r \int_R^r 3c\rho\Bigg[\theta\omega^2 r^2 + xR\omega^2 r + e_0 \omega r + \frac{\theta\mu^2 R^2 \omega^2}{2} + \frac{\mu R\omega f_1}{2}\Bigg] dr \, dr$$

Putting $e_0 = a_1 \mu R\omega/2$ and $b_1 = -a_1 r\omega$, and simplifying:

$$M_{T_s} = 3c\rho\omega^2\left[\theta C_r + (xR)B_r + \left(\frac{\theta\mu^2 R^2}{2}\right) A_r\right] \quad (25)$$

Part in cos Ψ:

$$M_{T_{\cos \Psi}} = \int_R^r \int_R^r 3c\rho[r\omega \, (e_1 \cos \Psi)] \, dr \, dr$$

Putting $e_1 = b_1 r\omega - a_0 \mu R\omega$

$$M_{T_{\cos \Psi}} = 3c\rho\omega^2[b_1 C_r - a_0 \mu R B_r] \cos \Psi \quad (26)$$

Part in sin Ψ:

$$M_{T_{\sin \Psi}} = \int_R^r \int_R^r 3c\rho(2\theta r R\mu\omega^2 + r\omega f_1 + \mu x R^2 \omega^2) \sin \Psi \, dr \, dr$$

Putting $f_1 = -r a_1 \omega$:

$$M_{T_{\sin \Psi}} = 3c\rho\omega^2[2\theta R\mu B_r - a_1 C_r + \mu x R^2 A_r] \sin \Psi \quad (27)$$

Part in cos 2Ψ:

$$M_{T_{\cos 2\Psi}} = \int_R^r \int_R^r 3c\rho \left[\frac{\theta(-\mu^2 R^2 \omega^2)}{2} + r\omega e_2 - \frac{\mu R \omega f_1}{2} \right] dr\, dr \cos 2\Psi$$

Putting $f_1 = -a_1 r\omega$ and $e_2 = a_1 \mu R\omega/2$:

$$M_{T_{\cos 2\Psi}} = 3c\rho\omega^2 \left[-\left(\frac{\mu^2 R^2 \theta}{2} \right) A_r + a_1 \mu R B_r \right] \cos 2\Psi \tag{28}$$

Part in sin 2Ψ:

$$M_{T_{\sin 2\Psi}} = \int_R^r \int_R^r 3c\rho [r\omega f_2 + (e_1/2)\mu R\omega]\, dr\, dr \sin 2\Psi$$

Putting $f_2 = (b_1/2)\mu R\omega$ and $e_1 = b_1 \omega r - a_0 \omega \mu R$

$$M_{T_{\sin 2\Psi}} = 3c\rho\omega^2 \left[-\left(\frac{a_0}{2} \mu^2 R^2 \right) A_r + b_1 \mu R B_r \right] \sin 2\Psi \tag{29}$$

Expression for Combined Effects of Centrifugal Force and Inertia

It should be noted that if Eqs. (6) and (8) are combined, the resultant value is $-m\omega^2 a_0 B_r$. That the resultant has the steady value $-m\omega^2 a_0 B_r$ can be shown in another way. Thus,

$$-m\omega^2 \beta B_r \; -m\ddot{\beta} B_r = -mB_r(\omega^2\beta + \ddot{\beta}) = mB_r\omega^2 a_0$$

$$\beta = a_0 - a_1 \cos\Psi - b_1 \sin\Psi$$

$$\ddot{\beta} = a_1 \cos\Psi\omega^2 + b_1 \sin\Psi\omega^2$$

Then,

$$\omega^2\beta + \ddot{\beta} = \omega^2(a_0 - a_1 \cos\Psi - b_1 \sin\Psi) + \omega^2(a_1 \cos\Psi + b_1 \sin\Psi) = \omega^2 a_0$$

It is therefore seen that the bending moment at any fixed point of the blade consists of three parts: (1) a steady part due to the combined effects of blade weight, centrifugal force, and inertia forces in flapping, (2) a steady part due to aerodynamic thrust, and (3) periodic parts due to aerodynamic thrust in cos Ψ, sin Ψ, cos 2Ψ and sin 2Ψ.

Effect of Ψ, the Azimuth Angle, on the Bending Moments at a Given Point on the Blade

One of the first problems that occur to the stress analyst lies in the value or values of Ψ which are likely to give the worst bending moment for given values of r/R and μ. In the calculations that follow r/R is taken as 0.5 and the value of μ as 0.4. These two values are selected as being especially typical. The results of these calculations are given in the curves of Fig. 1, in which terms in cos 2Ψ and sin 2Ψ are calculated with the alternative values a_1' and b_1'.

Subsidiary values from Table 1 for $\mu = 0.4$, $r/R = 0.5$, $R = 20$ are:

$A_r = 50$	$x = 0.0193$	$b_1 = 0.0630$
$B_r = 832$	$\omega = 20.6$	$m = 0.075$

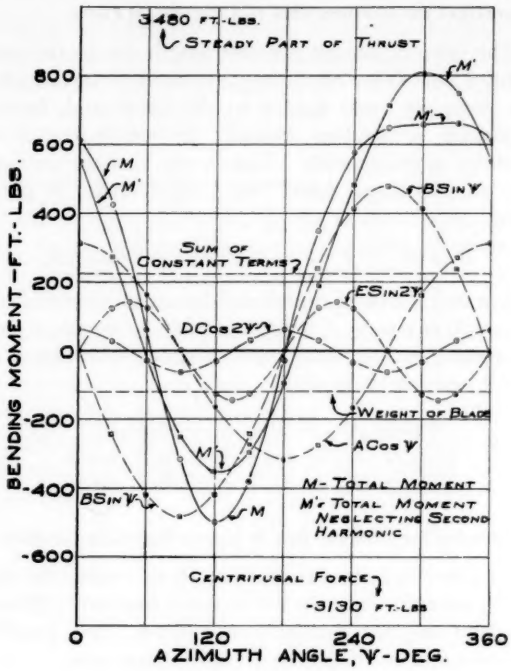

FIG. 1.

$C_r = 14.173$ $\quad a_0 = 0.1181$ $\quad a_1' = 0.0157$
$\theta = 0.0524$ $\quad a_1 = 0.0714$ $\quad b_1' = 0.03545$
$c = 1$ ft.

Steady terms—from Eqs. (4), (6) and (13), the steady terms are:

$$M_s = -mgA_r - m\omega^2 a_0 B_r + 3c\rho\omega^2 \times \left[\theta C_r + xRB_r + \left(\frac{\theta\mu^2 R^2}{2} \right) A_r \right] = -120.8 - 3{,}130 + 3{,}480 = 229$$

Terms in cos Ψ: From Eqs. (6), (8) and (14), the terms in cos Ψ are:

$$M_{\cos\Psi} = 3c\rho\omega^2[b_1 C_r - a_0 \mu R B_r] \cos\Psi = 324 \cos\Psi = A \cos\Psi$$

Terms in sin Ψ: From Eqs. (6), (8) and (15), the terms in sin Ψ are:

$$M_{\sin\Psi} = 3c\rho\omega^2[2\theta R\mu B_r - a_1 C_r + \mu x R^2 A_r] \sin\Psi = -482 \sin\Psi = B \sin\Psi$$

Terms in cos 2Ψ:

$$M_{\cos 2\Psi} = 3c\rho\omega^2 \left[-\left(\frac{\mu^2 R^2 \theta}{2} \right) A_r + a_1' \mu R B_r \right] \cos 2\Psi = 63 \cos 2\Psi = D \cos 2\Psi$$

Terms in sin 2Ψ:

$$M_{\sin 2\Psi} = 3c\rho\omega^2 \left[-\left(\frac{a_0}{2} \mu^2 R^2 \right) A_r + b_1' \mu R B_r \right] \sin 2\Psi = 142.5 \sin 2\Psi = E \sin 2\Psi$$

Effect of Ψ, the Azimuth Angle, on the Aerodynamic Thrust

It will be of interest to study the variation of aerodynamic thrust with the azimuth angle. The results are given in the curve of Fig. 2.

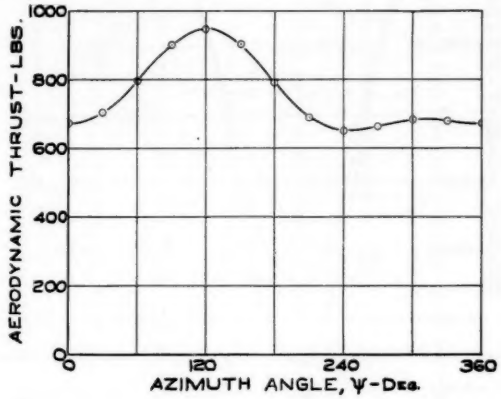

FIG. 2.

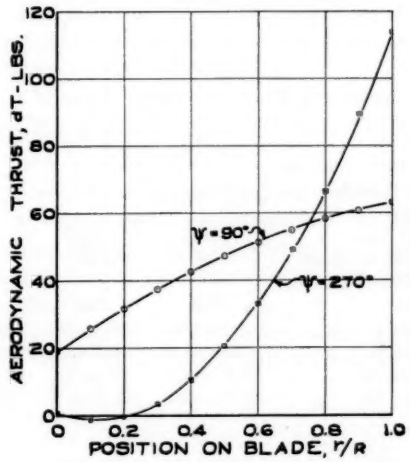

FIG. 3.

The complete expression for the aerodynamic thrust T_1 of a single blade, on which the above calculations are based is given by:

Steady terms:

$$C = 3c\rho\omega^2R^3\left[\frac{\theta}{3} + \frac{\theta\mu^2}{2} + \frac{x}{2}\right]$$

Terms in $\cos\Psi$:

$$A\cos\Psi = 3c\rho\omega^2R^3\left[\frac{b_1}{3} - \frac{a_0\mu}{2}\right]\cos\Psi$$

Terms in $\sin\Psi$:

$$B\sin\Psi = 3c\rho\omega^2R^3\left[\mu\theta - \frac{a_1}{3} + \mu x\right]\sin\Psi$$

Terms in $\cos 2\Psi$:

$$D\cos 2\Psi = 3c\rho\omega^2R^3\left[-\frac{\mu^2\theta}{2} + \frac{a_1'\mu}{2}\right]\cos 2\Psi$$

Terms in $\sin 2\Psi$:

$$E\sin 2\Psi = 3c\rho\omega^2R^3\left[\frac{b_1'\mu}{2} - \frac{a_0\mu^2}{2}\right]\sin 2\Psi$$

Variation of Aerodynamic Thrust with r/R

It is of interest now to study the affect of r/R on aerodynamic thrust. The results are given in the curves of Fig. 3.

An expression on which the above calculations can be conveniently based and in which terms are separated into a group independent of r, a group in r, and a group in r^2 is as follows:

$$dT = 3c\rho\left[\left(\frac{\theta\mu^2R^2\omega^2}{2} - \frac{\theta\mu^2R^2\omega^2\cos 2\Psi}{2} + \mu R^2\omega^2 x\sin\Psi - \frac{\mu^2R^2\omega^2a_0\sin 2\Psi}{2} + 2\theta R\mu\omega^2\sin\Psi + \omega^2xR - \omega^2a_0\mu R\cos\Psi + \frac{\omega^2a_1'\mu R\cos 2\Psi}{2}\right) + \left(\frac{\omega^2b_1'\mu R\sin 2\Psi}{2} + \frac{\mu R\omega^2b_1'\sin 2\Psi}{2} + \frac{\mu R\omega^2a_1'\cos 2\Psi}{2}\right)r + (\theta\omega^2 + \omega^2b_1\cos\Psi - \omega^2a_1\sin\Psi)r^2\right]dr$$

Discussion of the Effect of the Azimuth Angle Ψ on Bending Moments

From the curves of this section of the paper, the following conclusions emerge:

(1) As has long been known, but rarely set forth in mathematical terms, the bending moments for a rigid blade would be very high indeed. The steady term indicates a thrust moment at $r = 0.5R$ of 3,480 ft.lbs., which is reduced to only 229 ft.lbs. by the combined action of the blade weight and centrifugal force.

(2) The effect of second harmonic terms in the expression for the bending moment is neither negligible nor highly important.

(3) Contrary to the views of de la Cierva, it is not correct to neglect inertia effects and allow only for centrifugal force effects in computing bending moments. As might have been expected from the fact that the flapping moment is equivalent to a rotational motion about another axis, centrifugal force and inertia effects combined produce a bending moment that is independent of the azimuth angle Ψ.

(4) The constant positive bending moment (which is also the mean bending moment) is considerably smaller than the maximum positive bending moment and smaller numerically than the maximum negative bending moment.

(5) The maximum positive bending moment occurs on the retreating side at an azimuth angle of approximately 300 deg. from the rearmost position of the blade. The maximum negative bending moments occur on the advancing side at $\Psi = 120$ deg.

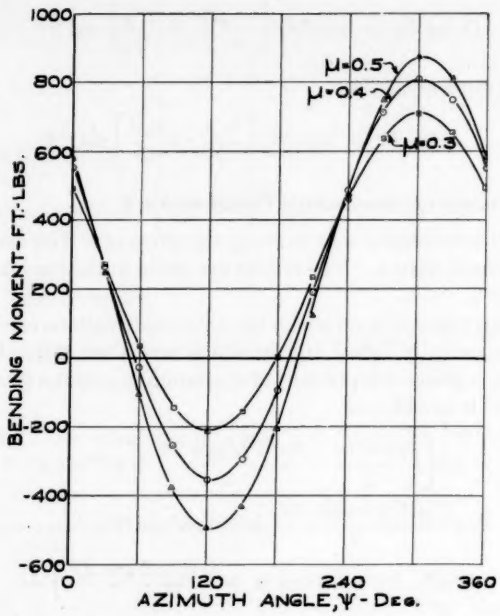

FIG. 4.

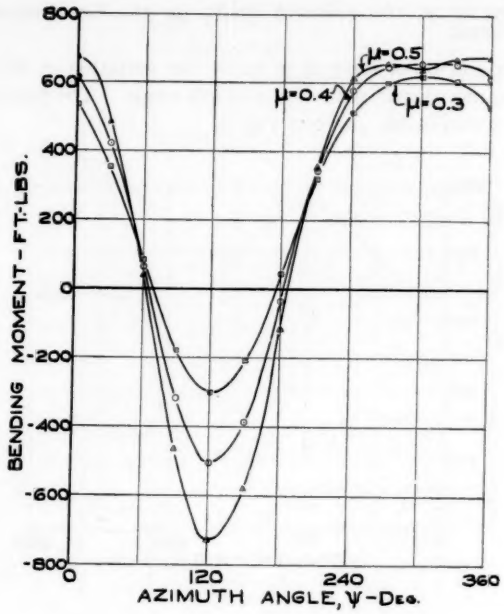

FIG. 5.

(6) While the thrust is greater on the advancing side than on the retreating side, the distribution of thrust (owing presumably to the flapping motion) is such that on the advancing side the thrust moves inboard; on the retreating side the thrust moves outboard.

(7) It is in this change of thrust distribution that lies the explanation of the changes in bending moment with the azimuth angle Ψ. On the advancing side, as the thrust moves inboard, the inertia effects and centrifugal force moments take charge and the bending moment becomes negative. On the retreating side the converse holds true.

EFFECT OF μ ON THE BENDING MOMENT AT A FIXED POINT ON THE BLADE

The qualitative argument regarding the effect of μ is as follows: At the higher values of V and μ, there is greater asymmetry of the flow, hence greater violence of flapping, greater inertia accelerations, etc. Therefore, at the higher values of μ greater variations in the bending moments at a given point on the blade might also be expected. For stress analysis purposes, it is evidently important to have an idea of the way in which bending moments vary with μ. Accordingly, the calculations under the heading "Effect of Ψ, the Azimuth Angle, ..." have been repeated with r/R held at 0.5, and μ taken as 0.3 and 0.5, with results given in Table 2 and Figs. 4 and 5.

Discussion of the Effect of μ on the Bending Moment

From the curves and calculation, the following may be concluded:

(1) The values of Ψ for which the maximum positive and negative bending moments occur are independent of the value of μ and remain at 300 and 120 deg., respectively.

(2) Increasing the value of μ progressively decreases the value of the constant or mean value of the bending.

(3) Increasing the value of μ has but a limited effect on the maximum positive bending moment but greatly increases the maximum negative bending moment.

TABLE 2

Moments in Ft.Lbs. for Various Values of μ

μ	0.3	0.4	0.5
Steady part due to weight of blade	−121	−121	−121
Steady part due to centrifugal force	−3190	−3130	−3045
Steady part of thrust	3,560	3,480	3,354
Total steady part of moment	249	229	188
Part in cos Ψ	245 cos Ψ	324 cos Ψ	394 cos Ψ
Part in sin Ψ	−390 sin Ψ	−482 sin Ψ	−562 sin Ψ
Part in cos 2Ψ	38.3 cos 2Ψ	63 sin Ψ	92.3 cos 2Ψ
Part in sin 2Ψ	81.2 sin 2Ψ	142.5 sin Ψ	215 sin 2Ψ

EFFECT OF THE RATIO r/R ON THE BENDING MOMENT

It was previously determined that for the point $r/R = 0.5$ the maximum positive bending moment occurred when $\mu = 0.5$ and $\Psi = 300$ deg. At the same value of $r/R = 0.5$ the maximum negative bending moment occurred when $\mu = 0.5$ and $\Psi = 180$ deg. In the section to follow it is proposed to investigate the effect of varying r/R, with $\mu = 0.5$ and Ψ given the two values as above. The results are shown in Fig. 6.

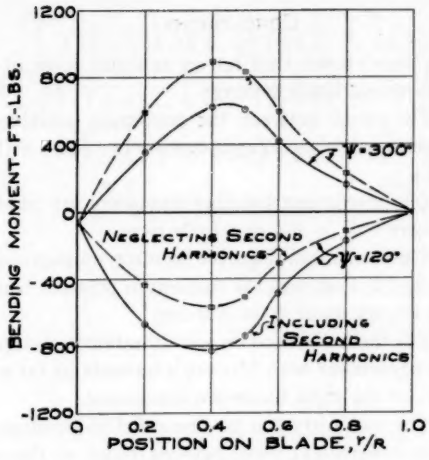

FIG. 6.

Discussion of the Effect of r/R on the Bending Moment

The main interest of the curves of Fig. 6 lies in the fact that at both $\Psi = 120$ deg. and $\Psi = 300$ deg. maximum values occur at $r/R = 0.4$. Thus, additional evidence is made available for the belief that for an autogiro rotor the maximum bending moments occur when r/R lies between 0.4 and 0.5.

FORMULAS FOR CENTRIFUGAL RELIEF OF BENDING MOMENTS

In reference 3 there is presented the derivation of a formula by Hohenemser, which, while it is based on some approximations, has far better physical and mathematical foundation that the empiric formulas available hitherto.

The formula for a blade of constant mass density and constant moment of inertia is found, after rather trying integrations, to be

$$M = \frac{M_{RG}}{1 + 0.052\ (R^2 CF_{r=0}/EI_s)} \qquad (30)$$

where

M_{RG} = bending moment of the blade which is hinged but rigid
M = bending moment of the blade with allowance for its elastic properties
R = blade radius in in.
$CF_{r=0}$ = centrifugal force at the point where the radius is zero
I_s = moment of inertia of the span in in.^{4}
E = modulus of elasticity in lbs. per sq.in.

It is interesting to investigate whether this formula is physically logical by the following qualitative argument.

(1) The actual moment $M = M_{RG}$ − moment due to centrifugal relief.

(2) The moment due to centrifugal relief $\approx CF_{r=0}y$, where y is the deflection.

(3) The deflection $y \approx \int\int(M\ dx\ dx/EI) \approx (MR^2/EI)$.

(4) Hence, $M = M_{RG} - K_1 CF_{r=0} MR^2/EI$ and $M = M_{RG}/[1 + (K_1 CF_{r=0} R^2/EI)]$ which has the same character of the analytic expression of Eq. (30).

Formula Presented in a Paper by Mulvey

In a paper by H. J. Mulvey[4] the following empiric formula is given for the maximum moment of an elastic or flexible blade, rectangular in chord and with constant mass distribution:

$$M = \left\{1/[1 + (12C''RT/Ba_0K)]\right\}\left\{\frac{C'RT}{B}\right\} \qquad (31)$$

In connection with this formula, the following assumptions are made:

(1) The maximum bending moment of the rigid blade occurs at 40 to 50 per cent of the blade radius.

(2) $C'RT/B$ represents the maximum bending moment in the plane of flapping of the rigid blade, R = radius, T = total thrust.

(3) The factor C' depends on the value of $V \sin \Psi/\omega R$ and has a maximum positive value for the retreating blade of $+0.04$ and a maximum negative value for the advancing blade of -0.06.

(4) The factor C'' depends on the mass distribution and has a value of 0.18 to 0.22 for conventional blade forms.

(5) K = a flexibility factor = $1{,}000/\tan^{-1}(2{,}000R/EI)$ where $\tan^{-1}(2{,}000R/EI)$ is in degrees and R is in ft.

(6) β_0 = average coning angle in degrees.

COMPARATIVE CALCULATIONS

It is interesting to compare the bending moments obtainable by Mulvey's formula and by the methods developed in this paper.

Maximum Bending Moments for the Rigid Blade

From Fig. 5 it is apparent that the maximum positive bending moment with $r/R = 0.5$ and $\mu = 0.5$ was 683 ft.lbs. with $\Psi = 0$ deg. The maximum negative bending moment is -830 ft.lbs. at $r/R = 0.4$ when $\Psi = 120$ deg. and $\mu = 0.5$, as seen in Fig. 6.

Mulvey's formula, Eq. (31), gives $C'RT/B = [(0.04)\ (20)\ (2275)]/3 = 606$ as the maximum positive bending moment and $[-(0.06)\ (20)\ (2275)]/3 = -910$ as the maximum negative bending moment. Thus, Mulvey's formula gives results close to those developed here.

Maximum Bending Moments with Allowance for Centrifugal Relief

With the use of Eq. (30)—for $\omega = 19.8$ (value of the angular velocity when $\mu = 0.5$) and $m = 0.075$:

$$CF_{r=0} = \frac{m\omega^2 R^2}{2} = 5{,}880 \text{ lbs.}$$

If E = 29,000,000 lbs. per sq.in., then I_s = 0.135 in.[4] The maximum positive bending moment of the elastic blade is given by

$$M = \frac{683}{1 + (0.052)\left(\frac{200^2 \times 5{,}880}{29{,}000{,}000 \times 0.135}\right)} = 124.5 \text{ ft.lbs.}$$

The maximum negative bending moment is given by

$$M = -830/5.49 = -142 \text{ ft.lbs.}$$

By Mulvey's formula, Eq. (31), the flexibility factor $K = 1{,}000/[\tan^{-1}(2{,}000R/EI_s)] = 1{,}716$.

$$\frac{12C''RT}{B} = 34{,}560 \text{ in.lbs.}$$

Then from Eq. (31)

$$M = \frac{606}{1 + (34{,}560/Ka_0)} = \frac{606}{1 + [34{,}560/(1{,}716)(7.14)]} = 160 \text{ ft.lbs.}$$

and the maximum negative bending moment

$$M = -910/3.8 = -227 \text{ ft.lbs.}$$

Conclusions

It has been shown that for an autogiro rotor of constant chord and blade setting:

(1) The range between the maximum positive and maximum negative bending moments increases with the value of μ.

(2) The maximum bending moments are likely to occur where $r/R = 0.4$ or a little over.

(3) The maximum negative bending moment occurs when $\Psi = 120$ deg. and the maximum positive bending moment occurs when $\Psi = 300$ deg.

(4) The method based on aerodynamic investigation is in fair agreement with Mulvey's formula as far as the moments of the rigid blade are concerned.

(5) The two formulas for the relief of bending moments by centrifugal force present relief of the same order of magnitude, but the relief factors are not in so close agreement as the moments for the rigid blade.

It is believed that the methods presented in this paper place the subject on a better basis than the purely empiric formulas generally employed and that the following further research is desirable: (a) extension of the methods to tapered autogiro blades; (b) application of the method to helicopter blades; (c) a closer examination of the problem of centrifugal relief.

References

[1] Glauert, H., *A General Theory of the Autogiro*, R. & M., No. 1111.

[2] Lock, C. N. H., *Further Development of Autogyro Theory*, R. & M., No. 1127.

[3] Hohenemser, K., *Performance of Rotating-Wing Aircraft*, N.A.C.A. T.M. No. 871, 28 pp., July, 1938; translated from Ingenieur-Archiv, Vol. 8, pp. 433–449, December, 1937.

[4] Mulvey, H. J., *Stress Analysis of Rotor Blades*, presented before the Institute of the Aeronautical Sciences, January, 1940.

Tension and Compression Stress-Strain Characteristics of Cold-Rolled Austenitic Chromium-Nickel and Chromium-Manganese-Nickel Stainless Steels

RUSSELL FRANKS* AND W. O. BINDER†

Union Carbide and Carbon Research Laboratories, Inc.

SYNOPSIS

The demand in recent years for lightweight high-strength structures, especially in the transportation industry, has created considerable interest in the corrosion-resisting chromium-nickel and chromium-manganese-nickel steels. These steels are austenitic in character, and their strength can be most economically increased by application of cold-work, which, together with composition, determines their ultimate mechanical properties. Data have been published on the cold-rolled chromium-nickel steels, but practically no information is available on the austenitic type of chromium-manganese-nickel steels. The present paper gives data on these latter steels. The effects of various degrees of cold-work on steels of different compositions are presented in order to describe those steels that have high strength associated with good ductility, which is important from the standpoint of fabrication of the sections required for lightweight high-strength construction.

The paper gives information on the stress-strain properties of the steels in both the longitudinal and transverse directions to rolling and shows the improvement obtained in these properties by application of the low temperature (200° to 300°C.) stress-relieving heat-treatment. It further shows that the 17 per cent chromium-7 per cent nickel steels, and the 17 per cent chromium-5.50 per cent manganese-4.50 per cent nickel steels have better tension and compression properties longitudinal to the direction of rolling than do the 18 per cent chromium-8 per cent nickel steels, particularly when the steels are cold-rolled to a tensile strength exceeding about 150,000 lbs. per sq.in. All these steels have better compressive properties transverse to the direction of rolling than longitudinal to the direction of rolling, but this difference is less marked in the 17 per cent chromium-7 per cent nickel steels and the 17 per cent chromium-5.50 per cent manganese-4.50 per cent nickel steels than in the 18 per cent chromium-8 per cent nickel steels. An attempt has been made to present the data on the steels so they will be of greatest value to the designer of lightweight high-strength structures.

THE PURPOSE OF THIS PAPER is to report briefly the results of an extended investigation on the stress-strain characteristics of the cold-rolled austenitic type of stainless steel, which has been applied in the construction of lightweight high-strength structures. The investigation has included a study of the stress-strain characteristics both in tension and compression. The well-established methods were used in studying the tension characteristics, but it was necessary to develop another procedure in order to determine the compressive properties of the relatively thin cold-rolled stainless steel strip. The details of this procedure have been published elsewhere,[1] and the importance of having satisfactory data about compressive properties has been emphasized by Aitchison and Tuckerman[2, 3] who stated that the strength of structures made of thin sections, such as in airplane wings and airplane fuselages, is generally limited by the strength of certain members carrying compressive loads, and unless such members are designed on the basis of compression it may lead to an unsafe or uneconomical structure. The method consists briefly of forming thin strip or sheet into cylinders having the proper slenderness ratio and diameter to thickness ratio so that when tested in compression they fail symmetrically to the axis. In the present paper only such reference will be made to the cylinder method as will aid in the discussion.

It should be emphasized that the strength of austenitic stainless steels can best be increased by application of cold-work. The extent of increase in strength is controlled by the amount of cold-work applied and the composition of the steel, as shown by Krivobok, et al.,[4] Lincoln,[5] and Bandel.[6] In view of the importance of these two factors, one of the principal objects of the investigation was to find steels in which the rate of work-hardening on cold-rolling was such that the resulting cold-rolled metal would have both high strength and good ductility in tension and in compression.

TESTING METHODS

The tensile experiments were made on samples from cold-rolled stainless steel strip approximately 0.035 in. thick in the longitudinal and transverse directions to rolling, using a standard-sized flat A.S.T.M. tensile specimen. The Berry gauge was employed with a 2-in. gauge length to obtain stress-strain data up to the 0.2 per cent offset* in tension. However, in determining the slopes of the modulus lines in tension, two metric Huggenberger gauges, Type A, were used, one on each side of the sample, and the stress-strain measurements

Presented at the Materials Session, Tenth Annual Meeting, I.Ae.S., New York, January 29, 1942.

* Research Metallurgist.

† Research Metallurgist.

* U.S. Navy Dept. Specification No. 47S21a for Steel, Corrosion-Resisting (18 per cent chromium-8 per cent nickel type) Sheet and Strip, Cold-Rolled, November 1, 1939.

TABLE 1

Effect of Different Percentages of Nickel on the Rate of Work Hardening of 18 and 17 Per Cent Chromium Steels*
All Steels Cold-Reduced 35 Per Cent

Heat No.	% Cr	% Ni	% C	Condition of metal	Tension†				Compression†	
					Initial tangent E in million lbs. per sq.in.	Yield strength 0.2% offset, lbs. per sq.in.	Tensile strength, lbs. per sq.in.	% Elongation in 2 in.	Rockwell "C" hardness	Initial tangent E in million lbs. per sq.in.	Yield strength 0.2% offset, lbs. per sq.in.
13	18.45	8.79	0.10	1	26	131,000	155,300	15	36	26	95,000
				3	27	155,000	173,400	11	37	27	118,000
E852	18.51	7.23	0.14	1	27	146,000	173,900	17	41	26	102,000
				2	27	151,000	174,400	14	41	27	132,000
E851	18.57	6.29	0.12	1	27	194,000	218,300	14	47	26	141,000
				2	28	196,000	218,000	13	47	27	168,000
E882	18.59	5.30	0.11	1	28	218,000	240,000	9	48	28	184,000
E880	17.39	8.11	0.11	1	27	144,000	179,800	15	40	25	116,000
				3	28	159,000	181,200	15	41	27	142,000
E717	17.15	7.17	0.11	1	26	164,000	196,000	15	43	26	139,000
				2	27	180,000	198,000	14	44	27	161,000
E850	17.45	6.28	0.12	1	28	195,000	229,500	14	48	26	171,000
				2	30	202,000	225,500	12	48	28	190,000
E881	17.51	5.31	0.12	1	28	230,000	245,000	5	50	26	208,000

* The steels contained from 0.50 to 1.32 per cent Mn and from 0.30 to 0.55 per cent Si.
† 0.035-in. thick strip tested longitudinal to direction of rolling.
1 = As cold-rolled.
2 = Cold-rolled, heated 72 hours at 200°C. and air-cooled.
3 = Cold-rolled, heated 24 hours at 275°C. and air-cooled.

were taken over a 2-cm. gauge length (0.787 in.). The 0.035-in. thick samples tested were 7 in. long and $^3/_4$ in. wide at the ends, with a $2^1/_2$-in. long reduced section $^1/_2$ in. wide. In testing for the yield strength at 0.2 per cent offset or for the slope of the modulus line using the Huggenberger gauges, loads were applied with a 60,000-lb. Baldwin Southwark Testing Machine, and sufficient time was allowed after application of each increment of load to permit the strain to be accurately measured. Without removal of the gauges the loads were applied beyond the elastic range into the plastic range until the yield strength at 0.20 per cent offset had been obtained. When this point was reached the strain gauges were removed and the samples were fractured.

The compression tests were made in both directions to rolling using the cylinder method. The samples employed in these tests were made from similarly cold-rolled stainless steel strip approximately 0.035 in. in thickness. In accordance with the requirement of the cylinder method the proper sized sections of the strip

TABLE 2

Data Obtained in Tension and Compression Tests on 0.035-In. Thick Strip of 18–8 Steel

Heat No.	% Cr	% Ni	% Mn	% Si	% C	% Cold-reduction	Condition of metal	Direction to rolling	Tension (C)†					Compression (D)‡			
									Initial tangent E in million lbs. per sq.in.	Proportional limit, lbs. per sq.in.	Yield strength 0.2% offset, lbs. per sq.in.	Tensile strength, lbs. per sq.in.	% Elongation in 2 in.	Rockwell "C" hardness	Initial tangent E in million lbs. per sq.in.	Proportional limit, lbs. per sq.in.	Yield strength 0.2% offset, lbs. per sq.in.	Buckling stress, lbs. per sq.in.
13	18.45	8.79	0.50	0.55	0.10	0	A	L	29	13,300	36,000	94,500	61	80*	28	11,000	36,000	50,250
						0	A	T	29	16,600	34,000	93,700	61		28	11,000	36,000	50,000
E716	17.60	8.87	1.16	0.37	0.11	20	1	L	27	21,000	121,000	139,300	22	29	26	23,700	74,000	120,400
						20	2	L	27	50,000	128,000	141,200	20	30	28	42,000	94,000	129,400
						20	1	T	28	40,000	113,000	138,500	17		27	36,900	121,000	145,000
						20	2	T	29	55,000	117,000	141,800	14		28	54,000	126,000	147,500
13	18.45	8.79	0.50	0.55	0.10	35	1	L	26	53,000	131,000	155,300	15	36	26	17,100	95,000	151,800
						35	2	L	27	60,000	155,000	173,400	11	37	27	47,600	118,000	158,000
						35	1	T	30	56,000	130,000	166,200	11		27	42,700	148,000	183,110
						35	2	T	31	56,000	147,000	178,700	10		29	72,000	169,000	193,000
E716	17.60	8.87	1.16	0.37	0.11	50	1	L	26	40,000	151,000	177,400	6	38	25	18,000	99,000	155,200
						50	2	L	27	63,000	167,000	187,000	5	40	26	43,000	129,000	168,200
						50	1	T	30	50,000	147,000	189,200	8		28	51,000	166,000	166,700
						50	2	T	31	53,000	164,000	198,300	6		29	65,000	183,000	211,000

* = Rockwell "B" value.
† C = Berry gauge data. Value for E based on Huggenberger gauge data.
‡ D = The 1.5-in. diameter cylinder tested had a slenderness ratio of 5 and a diameter to thickness ratio of 40.

A = Annealed.
1 = As cold-rolled.
2 = Cold-rolled, heated 72 hours at 200°C. and air-cooled.
L = Longitudinal to direction of rolling.
T = Transverse to direction of rolling.

were formed into cylinders with specially designed bending rolls that gave a sample, after machining, approximately $1\frac{1}{2}$ in. in diameter by 2 in. in length. The finished cylinder, which had a slenderness ratio of about 5 and a diameter to thickness ratio of about 40, was tested in compression using two Huggenberger extensometers of the metric type having a multiplication ratio of 1,175 to measure the strain. During test the proper increments of load were applied, and as before, sufficient time was allowed after application of each load to be sure that the correct strain value was observed. Loading was continued until the yield strength had been slightly exceeded, at which point the Huggenberger extensometers were removed and the loading was increased until failure occurred by uniform buckling near the ends of the sample. The compression properties of the strip were determined longitudinal or transverse to the direction of rolling depending upon the manner in which the cylinder was formed.

The proportional limit was determined by using the calculations of the stress-deviation method as a guide. The loading rate in tension and compression when using the Huggenberger gauges was about 2,000 lbs. per sq.-in. per min. and about 8,000 lbs. per sq.in. per min. when using the Berry gauge.

Certain of the tensile and compression samples were tested in the as-cold-rolled condition. Others were tested after heating at 200° to 300°C. (392° to 572°F.) 24 to 72 hours, followed by air cooling to observe the effect of the low temperature[7] stress-relieving heat-treatment on stress-strain characteristics.

Steels Tested

The materials included in this particular investigation consisted of steels that ranged in chromium content from about 16 to 20 per cent and in nickel content from about 5 to 10 per cent with up to 0.20 per cent carbon. All of the steels developed high strength on cold-rolling, but, as will be shown in the discussion of the results, certain of them had better ductility, and the properties of these will be discussed in detail. The properties of one of the steels of lower ductility as related to strength will also be discussed to illustrate the influence of composition on physical characteristics after cold-rolling.

As early as 1930 Becket[8] described the effects of manganese in promoting austenitic formation in steels containing 16 to 20 per cent chromium. His work showed that by the addition of 8 to 10 per cent manganese, steels containing 17 to 18 per cent chromium developed a structure consisting partly of austenite and partly of ferrite. These steels had good ductility and a high degree of corrosion resistance. Later on, in 1935, Becket, et al.,[9] described the effects of manganese and nickel jointly on steels of similar chromium content and showed that metal containing 17 to 18 per cent chromium, 5 to 6 per cent manganese and 4 to 5 per cent

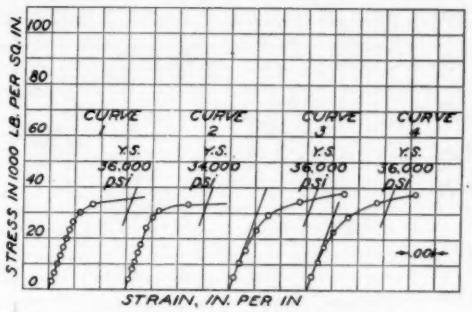

Fig. 1a. Reduced 0 per cent by cold-rolling, heat-treated at 1,050°C. Curve 1—Longitudinal to direction of rolling, tension. Curve 2—Transverse to direction of rolling, tension. Curve 3—Longitudinal to direction of rolling, compression. Curve 4—Transverse to direction of rolling, compression.

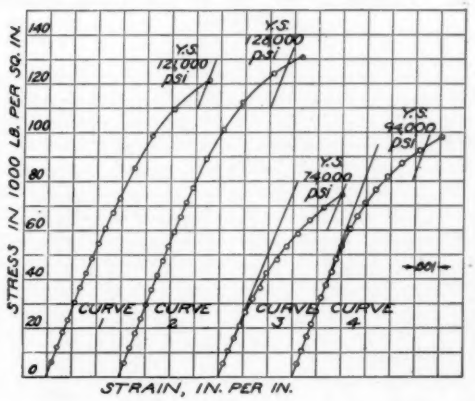

Fig. 1b. Reduced 20 per cent by cold-rolling, longitudinal direction.

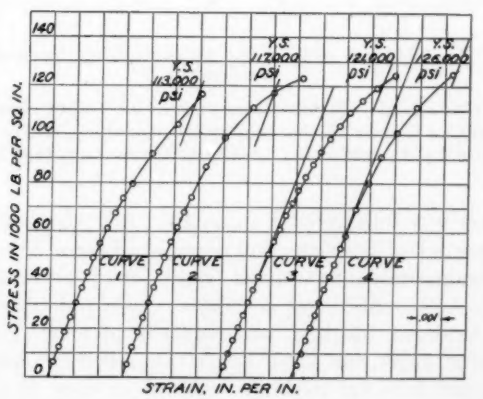

Fig. 1c. Reduced 20 per cent by cold-rolling, transverse direction.

Figs. 1b–1c. Curve 1—As cold-rolled, tension. Curve 2—As cold-rolled and heat-treated at 200°C., tension. Curve 3—As cold-rolled, compression. Curve 4—As cold-rolled and heat-treated at 200°C., compression.

Figs. 1a–1c. Stress-strain curves for 18 per cent chromium-8 per cent nickel steel.

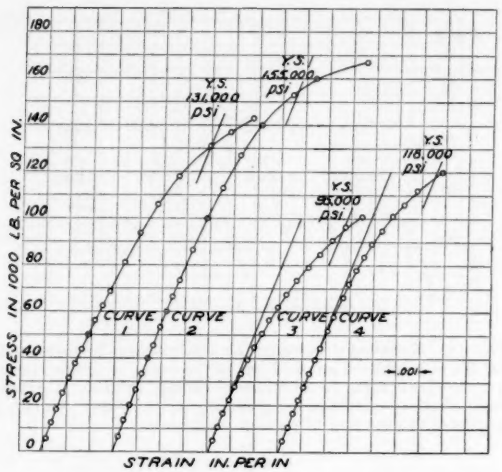

FIG. 2a. Reduced 35 per cent by cold-rolling, longitudinal direction.

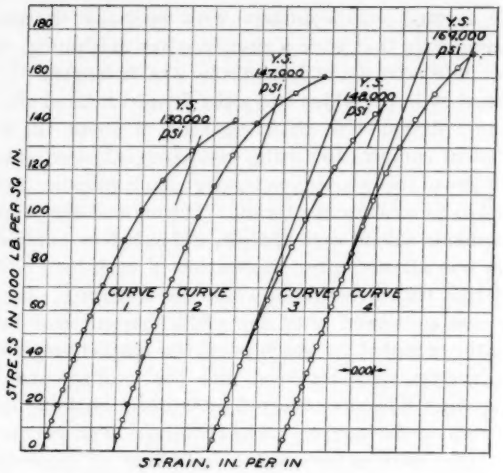

FIG. 2b. Reduced 35 per cent by cold-rolling, transverse direction.

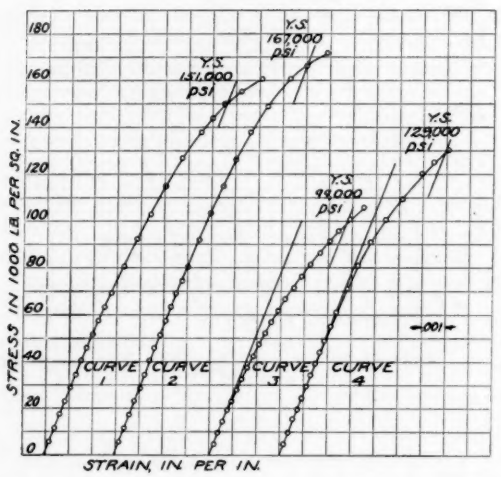

FIG. 2c. Reduced 50 per cent by cold-rolling, longitudinal direction.

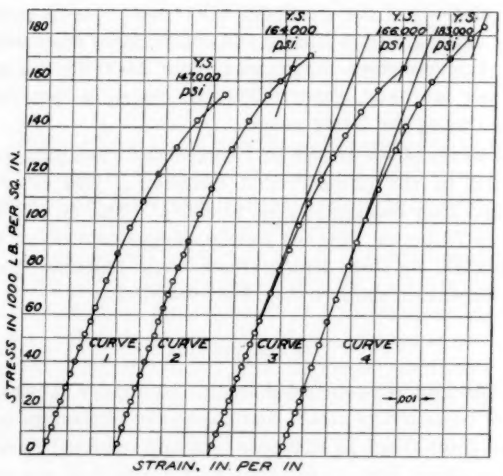

FIG. 2d. Reduced 50 per cent by cold-rolling, transverse direction.

FIGS. 2a–2d. Stress-strain curves for 18 per cent chromium-8 per cent nickel steel. Curve 1—As cold-rolled, tension. Curve 2—As cold-rolled and heat-treated at 200°C., tension. Curve 3—As cold-rolled, compression. Curve 4—As cold-rolled and heat-treated at 200°C., compression.

nickel was substantially austenitic. The stress-strain properties of both the chromium-manganese and the chromium-manganese-nickel steels after cold-rolling have been studied but nothing has been published on the subject. All these data cannot be presented in the present paper, but data on the cold-rolled chromium-manganese-nickel steel are included in view of their excellent stress-strain characteristics.

Discussion of Results

In order to determine the effect of cold-work as related to composition, the series of steels containing 17 and 18 per cent chromium, respectively, with about 8.5, 7, 6, and 5 per cent nickel and about 0.12 per cent carbon were given a 35 per cent cold-reduction by rolling to strip approximately 0.035 in. thick. The strips were tested in both tension and compression, and the data in the longitudinal direction to rolling are briefly summarized in Table 1.

The data show that the 18 per cent chromium steels containing 7, 6, and 5 per cent nickel have higher strength in both tension and compression than the 18 per cent chromium-8 per cent nickel steel because of their greater rate of work-hardening. The rate of work-hardening of the 5 per cent nickel steel may be considered to be too high in view of the relatively low ductility of the metal. Conversely, the rate of work-

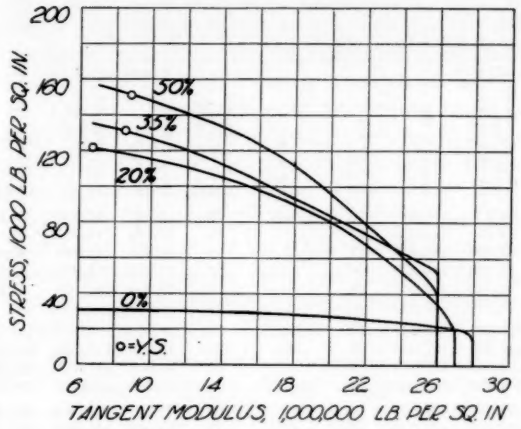

FIG. 3a. Tension, as cold-rolled.

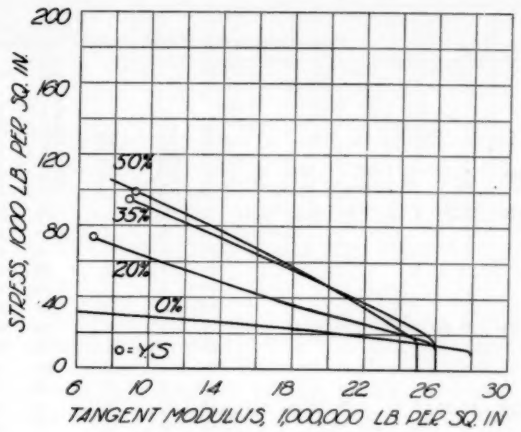

FIG. 3b. Compression, as cold-rolled.

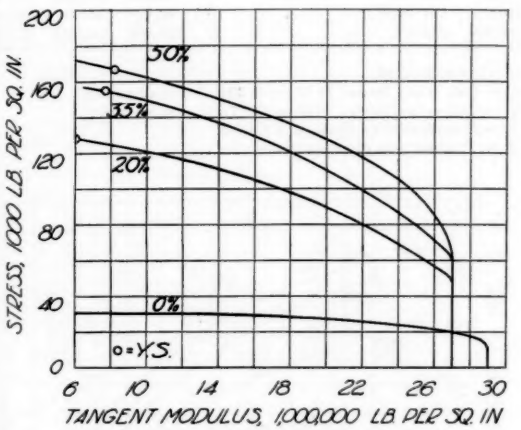

FIG. 3c. Tension, as cold-rolled and heat-treated at 200°C.

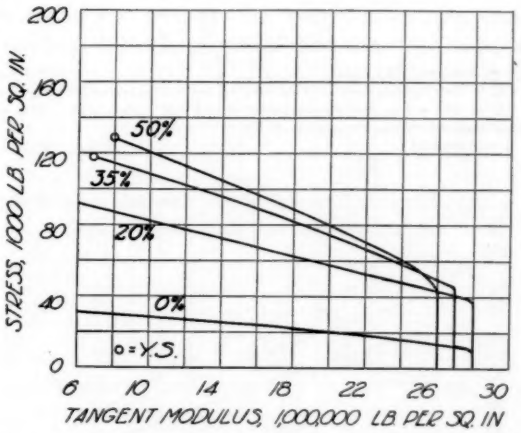

FIG. 3d. Compression, as cold-rolled and heat-treated at 200°C.

FIGS. 3a–3d. Tangent modulus curves derived from stress-strain curves for 18 per cent chromium-8 per cent nickel steel. Longitudinal to the direction of rolling.

hardening of the 18 per cent chromium-8 per cent nickel steel may be considered too low if high strength is required. The same general remarks apply for the 17 per cent chromium steels containing 8, 7, 6, and 5 per cent nickel with the exception that all of these steels are somewhat stronger than similar steels containing about 18 per cent chromium, indicating a higher rate of work-hardening for the 17 per cent chromium steels of comparable nickel content. It can also be said that the low-temperature heat-treatment at 200° to 300°C. (392° to 572°F.) improves the stress-strain characteristics of all these steels.

The testing was continued on cold-rolled strip (of the same thickness) of the 18 per cent chromium-8 per cent nickel and 17 per cent chromium-7 per cent nickel steels because these steels represented compositions with relatively slow and intermediate rates of work-hardening. The 18–8 steels were tested in the annealed condition and after cold-reducing in thickness 20, 35, and 50 per cent, respectively, while the 17 per cent chromium-7 per cent nickel steels were tested in the annealed condition and after cold-reducing by rolling, 10, 25, 35, and 40 per cent.

The data obtained in the tension and compression experiments on the 18–8 steel are given in Table 2, and the stress-strain data are shown in Figs. 1 and 2. Although the tensile strength of the 18–8 steel can be increased to about 180,000 lbs. per sq.in. by cold-reducing 50 per cent, the steel has a relatively low compressive yield strength (99,000 lbs. per sq.in.) at 0.2 per cent offset in the longitudinal direction to rolling and, in addition, the ductility is lower than expected. After 20 and 35 per cent cold-reduction the compressive yield strengths in the longitudinal direction to rolling are 74,000 and 96,000 lbs. per sq.in., respectively, showing that the compressive yield strength of the 18–8 steel in the longitudinal direction to rolling is not greatly raised by increasing the degree of cold-work beyond

TABLE 3

Data Obtained in Tension and Compression Tests on 0.035-In. Thick Strip of 17–7 Steel

Heat No.	% Cr	% Ni	% Mn	% Si	% C	% Cold-reduction	Condition of metal	Direction to rolling	Tension (C)† Initial tangent E in million lbs. per sq.in.	Tension (C)† Proportional limit, lbs. per sq.in.	Tension (C)† Yield strength 0.2% offset, lbs. per sq.in.	Tension (C)† Tensile strength, lbs. per sq.in.	Tension (C)† % Elongation in 2 in.	Tension (C)† Rockwell "C" hardness	Compression (D)‡ Initial tangent E in million lbs. per sq.in.	Compression (D)‡ Proportional limit, lbs. per sq.in.	Compression (D)‡ Yield strength 0.2% offset, lbs. per sq.in.	Compression (D)‡ Buckling stress, lbs. per sq.in.
E572	17.20	7.23	1.28	0.43	0.11	0	A	L	29	14,000	33,000	117,800	68	85*	28	12,000	40,000	57,800
						0	A	T	29	15,700	33,000	113,500	62		29	12,000	44,000	57,400
						10	1	L	28	16,700	67,000	147,600	47	32	27	12,600	54,000	89,400
						10	2	L	28	20,000	65,000	140,900	56	32	27	21,000	64,000	89,700
						10	1	T	28	21,100	72,000	147,100	36		27	22,800	81,000	97,700
						10	2	T	28	27,000	74,000	140,800	43		27	25,700	74,000	102,000
21	17.33	7.14	1.29	0.37	0.13	25	1	L	28	22,000	127,000	165,200	24	38	26	16,000	96,000	151,400
						25	3	L	29	36,000	142,000	167,000	23	39	28	48,000	119,000	156,100
						25	1	T	30	45,000	124,000	170,500	17		28	43,000	143,000	172,200
						25	3	T	30	60,000	134,000	167,200	18		29	54,000	154,000	177,500
E717	17.15	7.17	1.32	0.34	0.11	35	1	L	26	50,000	164,000	196,000	15	43	26	29,700	139,000	184,500
						35	2	L	27	53,000	180,000	198,000	14	44	27	62,000	161,000	201,200
						35	1	T	30	46,400	138,000	201,000	10		27	47,000	185,000	214,300
						35	2	T	30	61,000	170,000	202,000	10		29	65,000	200,000	218,500
						45	1	L	27	48,000	200,000	225,000	7	46	26	27,000	163,000	218,000
						45	2	L	28	60,000	215,000	235,000	5	47	27	65,000	193,000	230,000
						45	1	T	31	56,000	176,000	234,000	7		29	64,000	230,000	250,000
						45	2	T	31	76,000	196,000	232,000	5		30	120,000	252,000	272,000

* = Rockwell "B" value.

† C = Berry gauge data. Value for E based on Huggenberger gauge data.

‡ D = The 1.5-in. diameter cylinder tested had a slenderness ratio of 5 and a diameter to thickness ratio of 40.

A = Annealed.

1 = As cold-rolled.

2 = Cold-rolled, heated 72 hours at 200°C. and air-cooled.

3 = Cold-rolled, heated 24 hours at 275°C. and air-cooled.

L = Longitudinal to direction of rolling.

T = Transverse to direction of rolling.

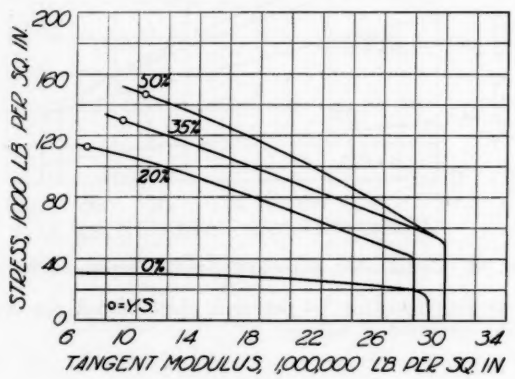

FIG. 4a. **Tension,** as cold-rolled.

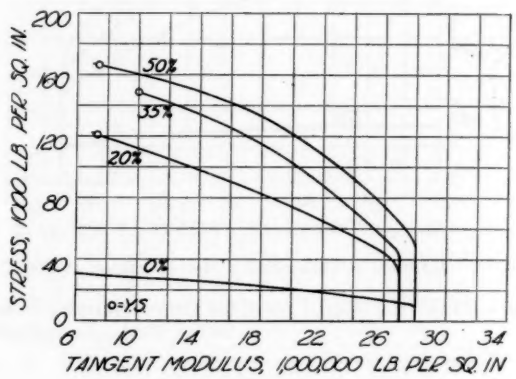

FIG. 4b. **Compression,** as cold-rolled.

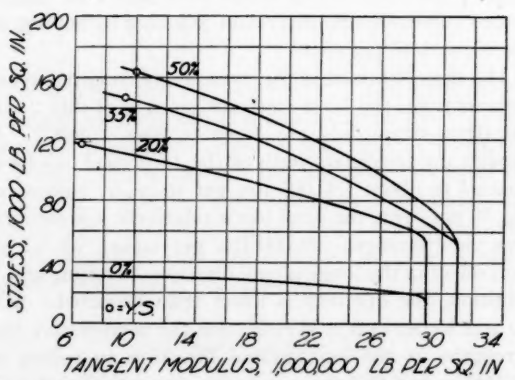

FIG. 4c. Tension, as cold-rolled and heat-treated at 200°C.

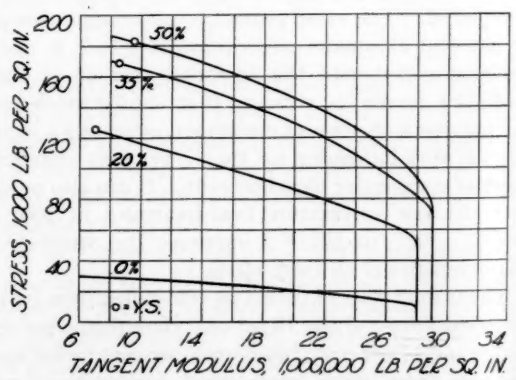

FIG. 4d. Compression, as cold-rolled and heat-treated at 200°C.

FIGS. 4a–4d. Tangent modulus curves derived from stress-strain curves for 18 per cent chromium-8 per cent nickel steel. Transverse to the direction of rolling.

20 per cent. The 18–8 steel exhibits much better compressive properties in the transverse direction to rolling. This is clearly illustrated by the tangent modulus curves of Figs. 3 and 4, which, like the stress-strain curves of Figs. 1 and 2, effectively show the improvement obtained by the low temperature heat-treatment at 200° to 300°C. (392° to 572°F.) after application of different percentages of cold-work.

As previously indicated, the effect of cold-work in increasing the strength of the 17 per cent chromium-7 per cent nickel steel is far more pronounced. The data for this steel after different percentages of cold-reduction are given in Table 3 and are represented by the stress-strain curves of Figs. 5, 6, and 7. It is at once observed that the tensile strength of this steel can be increased to about 200,000 lbs. per sq.in. by cold reducing 35 per cent and that with this tensile strength the steel has a relatively high compressive yield strength, at 0.2 per cent offset, in the longitudinal direction to rolling. The steel also has good ductility. At lower tensile strengths the steel has a comparatively high yield strength in compression in the longitudinal direction, but, as in the case of the 18–8 steel, there is a difference in the tension and compression stress-strain properties in the longitudinal direction to rolling, and this difference should be taken into consideration in de-

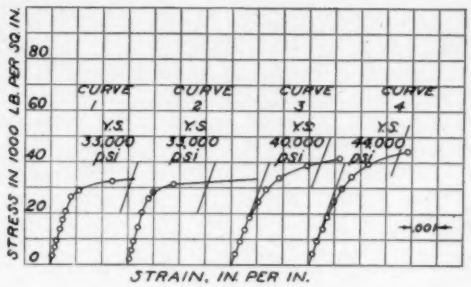

FIG. 5. Stress-strain curves for 17 per cent chromium-7 per cent nickel steel. Reduced 0 per cent by cold-rolling, heat-treated at 1,050°C. Curve 1—Longitudinal to direction of rolling, tension. Curve 2—Transverse to direction of rolling, tension. Curve 3—Longitudinal to direction of rolling, compression. Curve 4—Transverse to direction of rolling, compression.

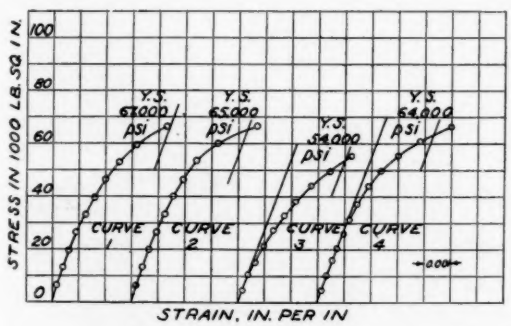

FIG. 6a. Reduced 10 per cent by cold-rolling, longitudinal direction.

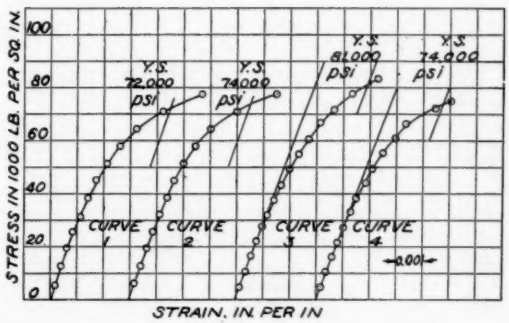

FIG. 6b. Reduced 10 per cent by cold-rolling, transverse direction.

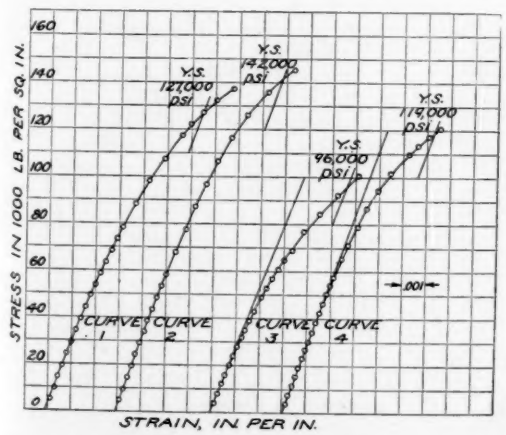

FIG. 6c. Reduced 25 per cent by cold-rolling, longitudinal direction.

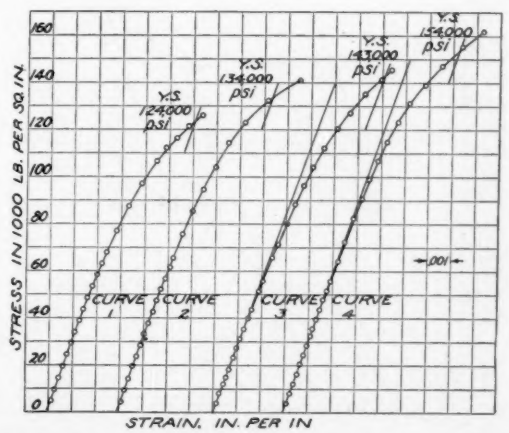

FIG. 6d. Reduced 25 per cent by cold-rolling, transverse direction.

FIGS. 6a–6d. Stress-strain curves for 17 per cent chromium-7 per cent nickel steel. Curve 1—As cold-rolled, tension. Curve 2—As cold-rolled and heat-treated at 200°–275°C., tension. Curve 3—As cold-rolled, compression. Curve 4—As cold-rolled and heat-treated at 200°–275°C., compression.

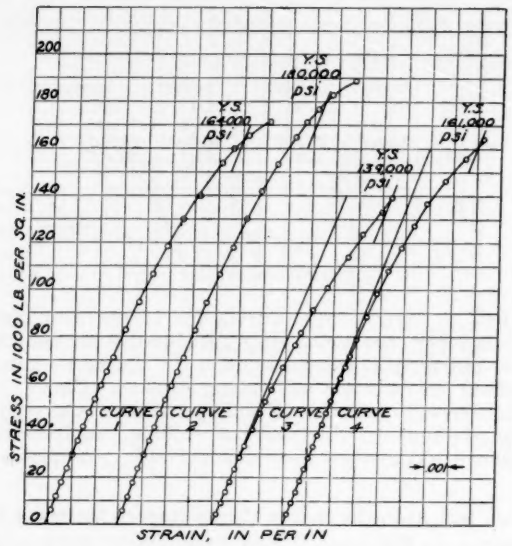

FIG. 7a. Reduced 35 per cent by cold-rolling, longitudinal direction.

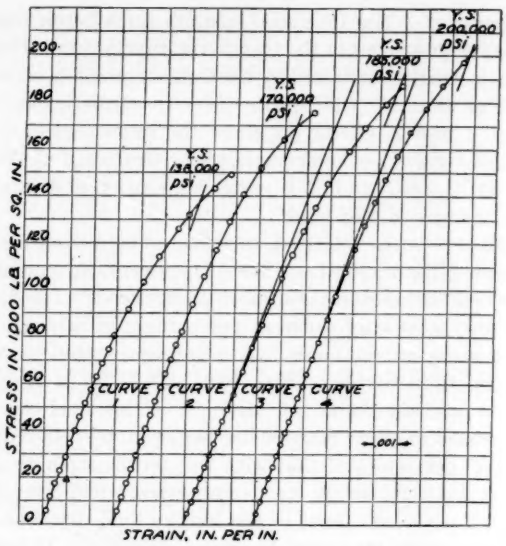

FIG. 7b. Reduced 35 per cent by cold-rolling, transverse direction.

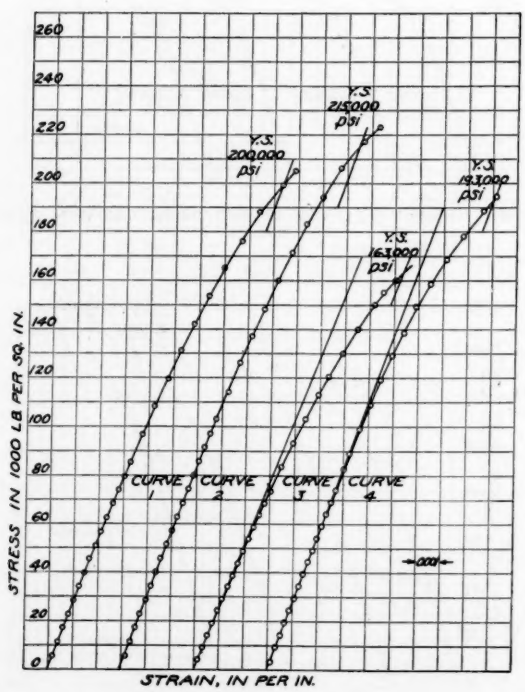

FIG. 7c. Reduced 45 per cent by cold-rolling, longitudinal direction.

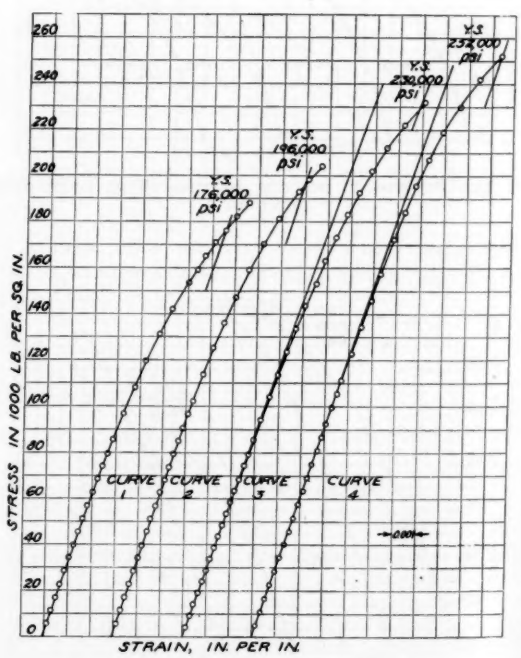

FIG. 7d. Reduced 45 per cent by cold-rolling, transverse direction.

FIGS. 7a–7d. Stress-strain curves for 17 per cent chromium-7 per cent nickel steel. Curve 1—As cold-rolled, tension. Curve 2—As cold-rolled and heat-treated at 200°–275°C., tension. Curve 3—As cold-rolled, compression. Curve 4—As cold-rolled and heat-treated at 200°–275°C., compression.

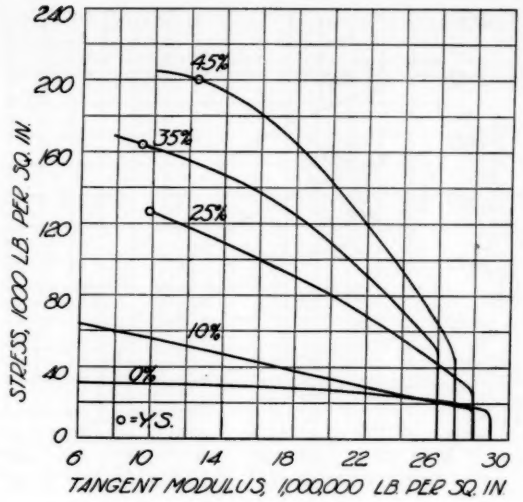

FIG. 8a. Tension, as cold-rolled.

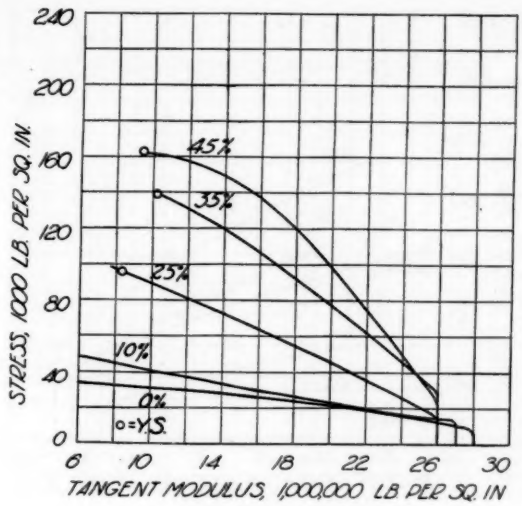

FIG. 8b. Compression, as cold-rolled.

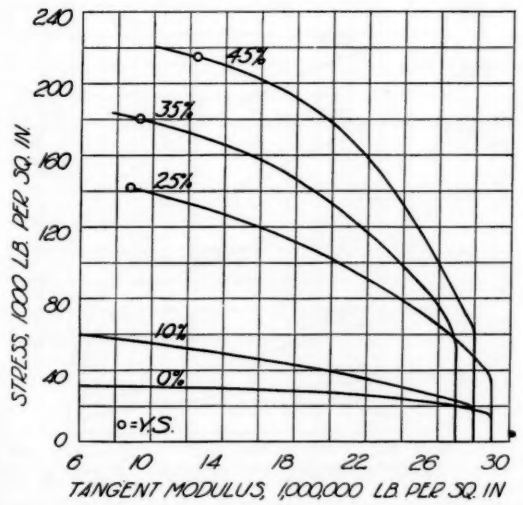

FIG. 8c. Tension, as cold-rolled and heat-treated at 200°–275°C.

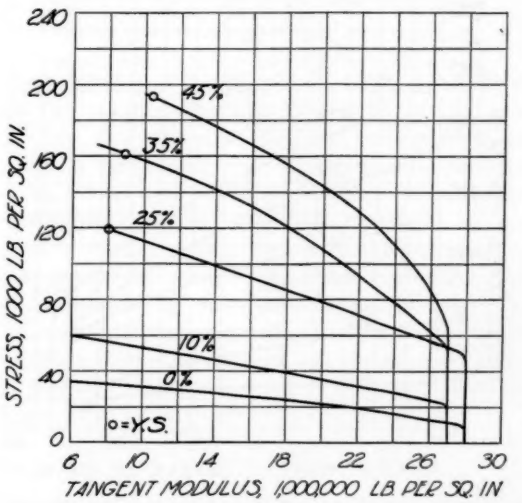

FIG. 8d. Compression, as cold-rolled and heat-treated at 200°–275°C.

FIGS. 8a–8d. Tangent modulus curves derived from stress-strain curves for 17 per cent chromium-7 per cent nickel steel. Longitudinal to the direction of rolling.

signing structures of the steel. The tangent modulus curves of Figs. 8 and 9 show the difference in the longitudinal tension and compression properties and also the difference in the longitudinal and transverse properties in both tension and compression. It is apparent from these curves that in the transverse direction the 17–7 steel has exceedingly high compression properties. The improvement obtained by the low-temperature stress-relieving heat-treatment is again in evidence for the properties in both directions to rolling.

As shown by the data in Table 4, the remaining steel included in the discussion contains approximately 17.50 per cent chromium, 5.50 per cent manganese, 4.50 per cent nickel and 0.12 per cent carbon. This steel was tested in the annealed condition and after cold-reducing 15, 25, and 35 per cent. The stress-strain data are presented in Figs. 10 and 11, and the tangent modulus curves in Figs. 12 and 13. It should be noted that the tensile strength of this steel is readily increased by cold-rolling and that after stress-relieving at 225°C. (440°F.) the cold-rolled strip has approximately the same yield strength in tension as in compression in the longitudinal direction to rolling. This is considered to be an advantage. The data further show that the steel has a high ductility which is retained after stress-relieving even though a marked improvement, as revealed by the tangent modulus curves, is obtained in the stress-strain characteristics. Like the

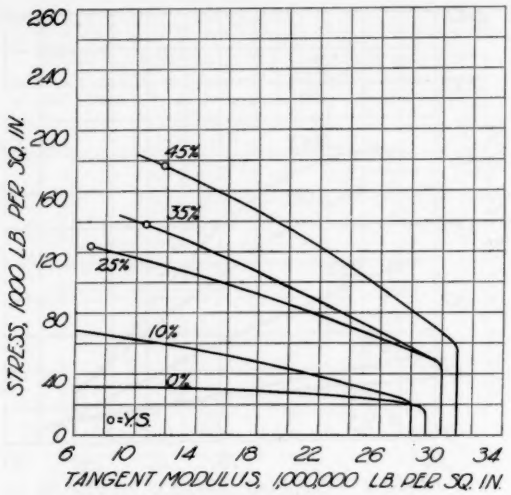

FIG. 9a. Tension, as cold-rolled.

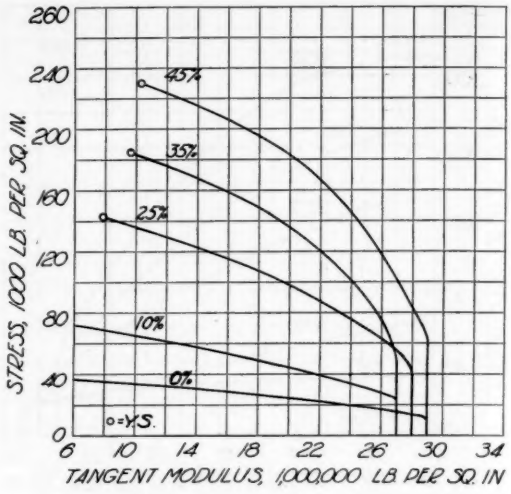

FIG. 9b. Compression, as cold-rolled.

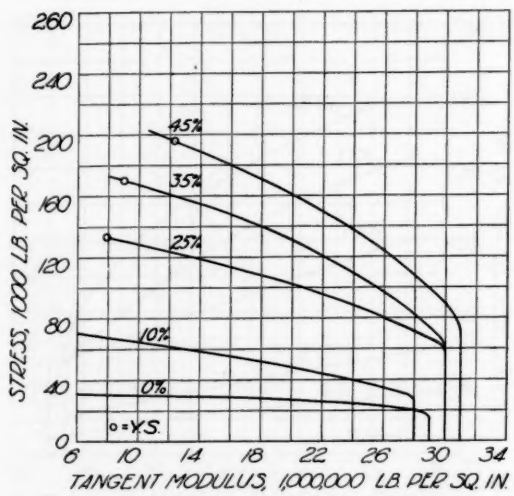

FIG. 9c. Tension, as cold-rolled and heat-treated at 200°–275°C.

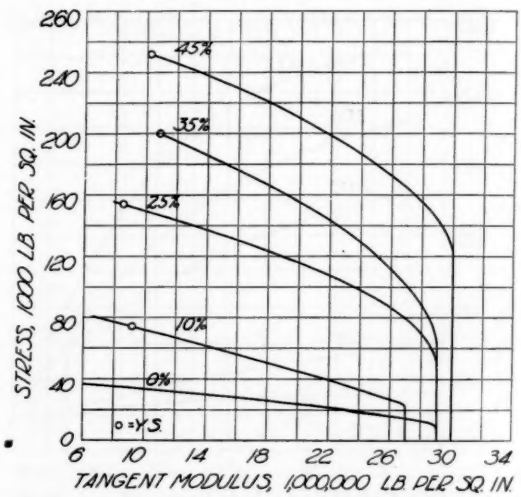

FIG. 9d. Compression, as cold-rolled and heat-treated at 200°–275°C.

FIGS. 9a–9d. Tangent modulus curves derived from stress-strain curves for 17 per cent chromium-7 per cent nickel steel. Transverse to the direction of rolling.

cold-rolled 18 per cent chromium-8 per cent nickel and the 17 per cent chromium-7 per cent nickel steels, the chromium-manganese-nickel steel exhibits the higher resistance to compressive stress in the transverse direction. The comparison may be carried further with the statement that the cold-rolled chromium-manganese-nickel steel has superior physical properties to the 18–8 steel and is at least equal in this respect to the 17–7 steel.

A few remarks should be made in regard to the corrosion resistance of the chromium-manganese-nickel steel. While the steel has not been used widely under commercial conditions in this country, tests made on it show that it has satisfactory resistance to staining in the atmosphere. The steel successfully resists other types of corrosion and in general is considered comparable to the 17 per cent chromium and 7 per cent nickel steel.

The curves of Figs. 14 to 19, inclusive, make possible a further study of the properties of the 18 per cent chromium-8 per cent nickel, the 17 per cent chromium-7 per cent nickel, and the 17 per cent chromium-5.50 per cent manganese and 4 per cent nickel steels. These curves have been constructed using different stress levels and simultaneously taking into consideration the tangent modulus and the percentage of cold-work applied to the steels. They show, in the first place, that the 17 per cent chromium-7 per cent nickel and the 17 per cent chromium–5.50 per cent manganese, and 4 per cent nickel steels are approximately equal in

TABLE 4

Data Obtained in Tension and Compression Tests on 0.035-In. Thick Strip of Chromium-Manganese-Nickel Steel

									Tension (C)†					Compression (D)‡			
Heat No.	% Cr	% Ni	% Mn	% Si	% C	% Cold-reduction	Condition of metal	Direction to rolling	Initial tangent E in million lbs. per sq.in.	Proportional limit, lbs. per sq. in.	Yield strength 0.2% offset, lbs. per sq.in.	Tensile strength, lbs. per sq.in.	% Elongation in 2 in.	Rockwell "C" hardness	Initial tangent E in million lbs. per sq.in.	Proportional limit, lbs. per sq.in.	Yield strength at 0.2% offset, lbs. per sq.in.	Buckling stress, lbs. per sq.in.
H194	17.52	4.34	5.43	0.27	0.12	0	A	L	29	25,500	40,700	138,500	65	90*	29	15,000	48,000	70,200
H194	17.52	4.34	5.43	0.27	0.12	0	A	T	29	25,500	41,000	141,500	62		29	10,000	48,000	70,300
H194	17.52	4.34	5.43	0.27	0.12	15	1	L	28	30,000	85,000	170,500	37	30	26	14,800	68,000	118,800
H194	17.52	4.34	5.43	0.27	0.12	15	2	L	28	30,000	84,000	165,100	46	30	27	25,000	85,000	121,400
H194	17.52	4.34	5.43	0.27	0.12	15	1	T	28	31,100	83,000	162,000	33		26	23,600	98,000	125,300
H194	17.52	4.34	5.43	0.27	0.12	15	2	T	28	34,000	94,000	154,100	40		27	37,000	101,000	129,800
H194	17.52	4.34	5.43	0.27	0.12	25	1	L	27	34,100	119,000	183,000	25	40	26	18,300	102,000	160,000
H194	17.52	4.34	5.43	0.27	0.12	25	2	L	28	34,100	133,000	179,500	32	40	27	38,200	127,000	165,000
H194	17.52	4.34	5.43	0.27	0.12	25	1	T	29	44,000	109,000	199,500	14		26	39,900	146,000	174,700
H194	17.52	4.34	5.43	0.27	0.12	25	2	T	29	45,000	132,000	173,500	17		28	56,000	150,000	176,000
H194	17.52	4.34	5.43	0.27	0.12	35	1	L	28	33,000	157,000	213,000	19	45	26	28,700	140,000	192,500
H194	17.52	4.34	5.43	0.27	0.12	35	2	L	28	54,000	182,000	203,500	18	45	27	57,400	168,000	202,000
H194	17.52	4.34	5.43	0.27	0.12	35	1	T	31	40,000	137,000	215,000	10		28	48,800	193,000	218,700
H194	17.52	4.34	5.43	0.27	0.12	35	2	T	31	52,000	171,000	207,000	10		29	95,000	207,000	228,600

* = Rockwell "B" value.

† C = Berry gauge. Value for E based on Huggenberger gauge data.

‡ D = The 1.5-in. diameter cylinder tested had a slenderness ratio of 5 and a diameter to thickness ratio of 40.

A = annealed.
1 = As cold-rolled.
2 = As cold-rolled, heated 24 hours at 225°C. and air-cooled.
L = Longitudinal to the direction of rolling.
T = Transverse to the direction of rolling.

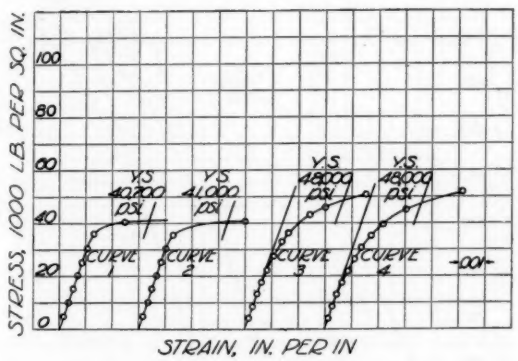

FIG. 10a. Reduced 0 per cent by cold-rolling, heat-treated at 1,050°C. Curve 1—Longitudinal to direction of rolling, tension. Curve 2—Transverse to direction of rolling, tension. Curve 3—Longitudinal to direction of rolling, compression. Curve 4—Transverse to direction of rolling, compression.

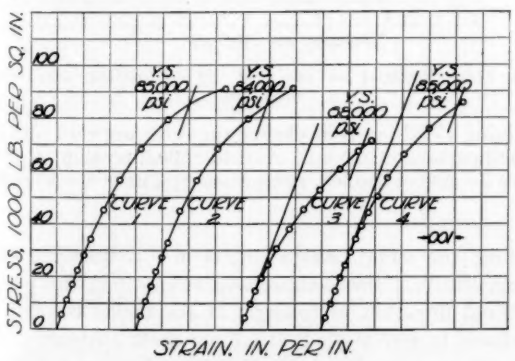

FIG. 10b. Reduced 15 per cent by cold-rolling, longitudinal direction.

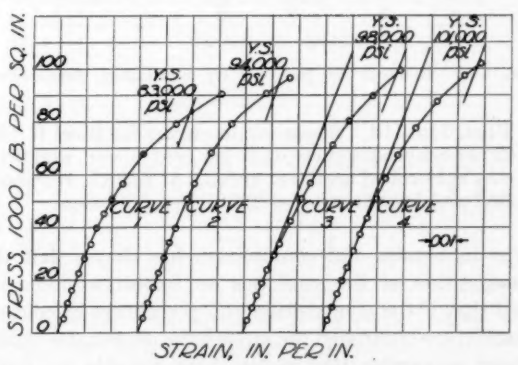

FIG. 10c. Reduced 15 per cent by cold-rolling, transverse direction.

FIGS. 10b–10c. Curve 1—As cold-rolled, tension. Curve 2—As cold-rolled and heat-treated at 225°C., tension. Curve 3—As cold-rolled, compression. Curve 4—As cold-rolled and heat-treated at 225°C., compression.

FIGS. 10a–10c. Stress-strain curves for Steel H194 containing 17.52 per cent chromium, 4.34 per cent nickel, 5.43 per cent manganese, 0.27 per cent silicon, and 0.12 per cent carbon.

tensile strength after cold-working to the same degree, with the exception that after 25 and 35 per cent cold-reduction the chromium-manganese-nickel steel has somewhat higher compressive properties in the longitudinal direction to rolling, particularly when the low temperature stress-relieving heat-treatment is employed. A study of these curves reveals the improvement secured by application of the low-temperature heat-treatment and the superiority of the cold-rolled 17–7 and chromium-manganese-nickel steels over the cold-rolled 18–8 steel for resisting deformation under high stresses. It is believed that these curves permit ready interpretation of the stress-strain data.

SUMMARY

The study of the effect of cold-work on the stress-strain characteristics of stainless steels of the austenitic

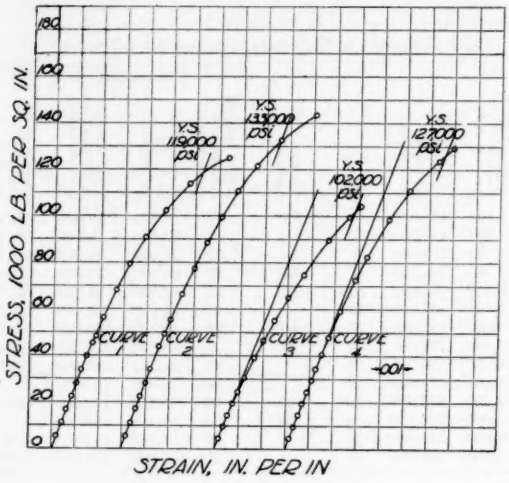

FIG. 11a. Reduced 25 per cent by cold-rolling, longitudinal direction.

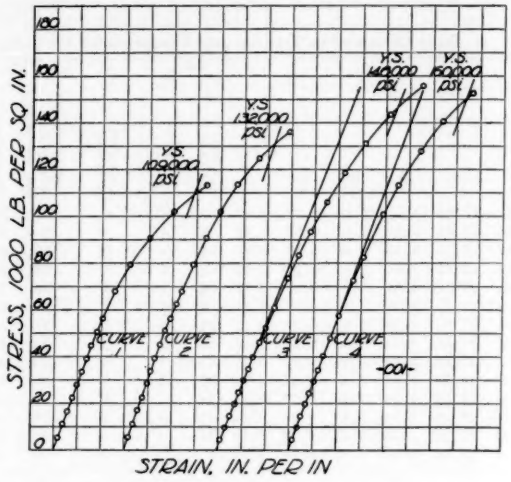

FIG. 11b. Reduced 25 per cent by cold-rolling, transverse direction.

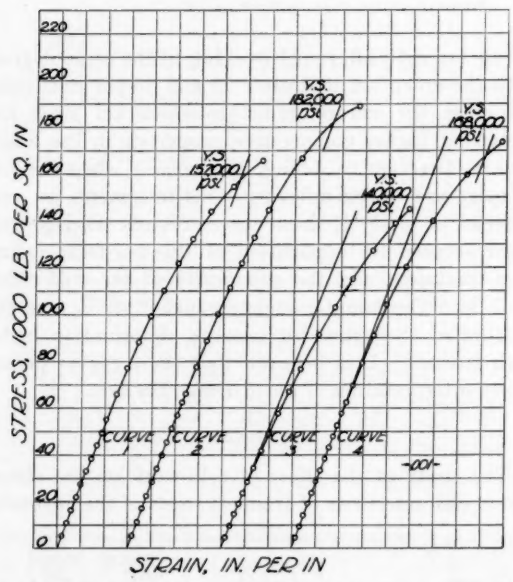

FIG. 11c. Reduced 35 per cent by cold-rolling, longitudinal direction.

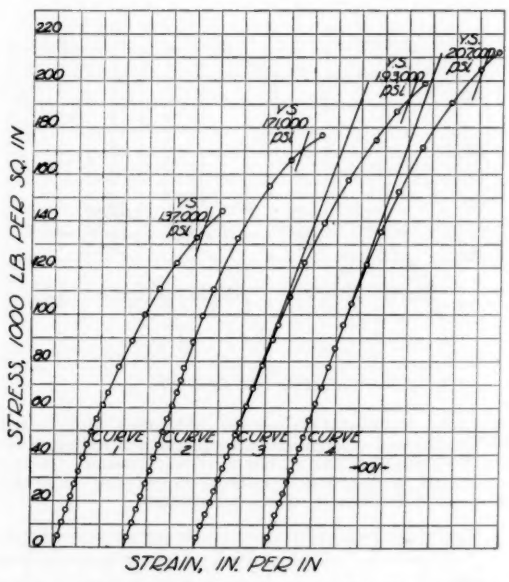

FIG. 11d. Reduced 35 per cent by cold-rolling, transverse direction.

FIGS. 11a–11d. Stress-strain curves for Steel H194 containing 17.52 per cent chromium, 4.34 per cent nickel, 5.43 per cent manganese, 0.27 per cent silicon, and 0.12 per cent carbon. Curve 1—As cold-rolled, tension. Curve 2—As cold-rolled and heat-treated at 225°C., tension. Curve 3—As cold-rolled, compression. Curve 4—As cold-rolled and heat-treated at 225°C., compression.

type in tension and compression has shown that the composition of the steel has an important influence and that if the composition and percentage of cold-reduction are controlled the steels have predictable stress-strain properties that make them suitable for light-weight high-strength construction.

If the chromium-nickel steel is fully austenitic, its rate of work-hardening on cold-rolling is relatively slow, and it is impractical to obtain tensile strengths of 200,000 lbs. per sq.in. or higher without excessively cold-rolling the metal, which results in low ductility and comparatively low compressive strength in the longitudinal direction to rolling. If the nickel content is reduced to give steels that are not quite austenitic, the rate of work-hardening is neither too fast nor too slow, and high strength with good ductility is obtained.

Cold-rolled steels in which high strength and good ductility are obtainable are those that contain 16 to 18 per cent chromium and about 7 per cent nickel with 0.10 to 0.16 per cent carbon. Similarly, good proper-

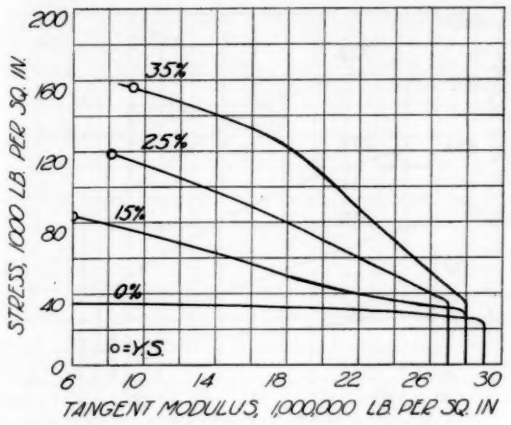

FIG. 12a. Tension, as cold-rolled.

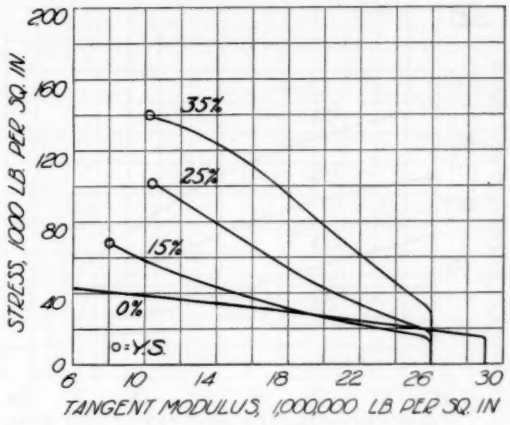

FIG. 12b. Compression, as cold-rolled.

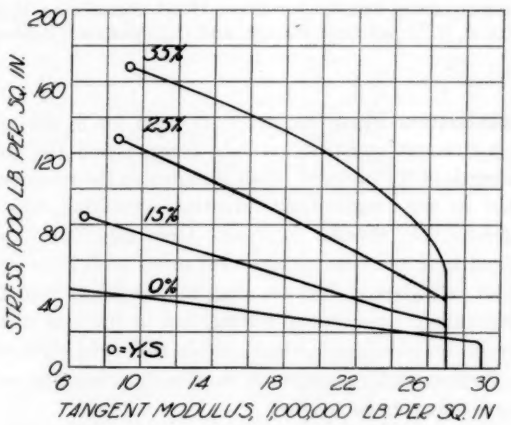

FIG. 12c. Tension, as cold-rolled and heat-treated at 225°C.

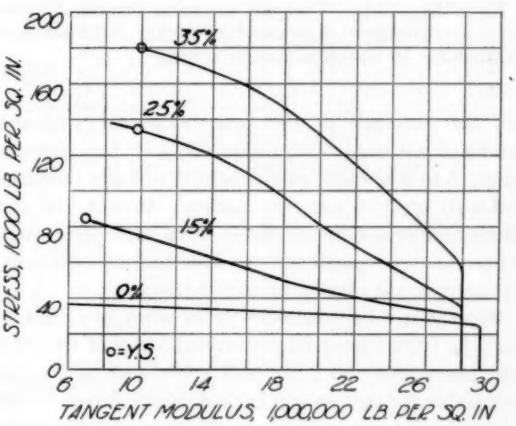

FIG. 12d. Compression, as cold-rolled and heat-treated at 225°C.

FIGS. 12a–12d. Tangent modulus curves derived from stress-strain curves for Steel H194 containing 17.52 per cent chromium, 4.34 per cent nickel, 5.43 per cent manganese, 0.27 per cent silicon, and 0.12 per cent carbon. Longitudinal to the direction of rolling.

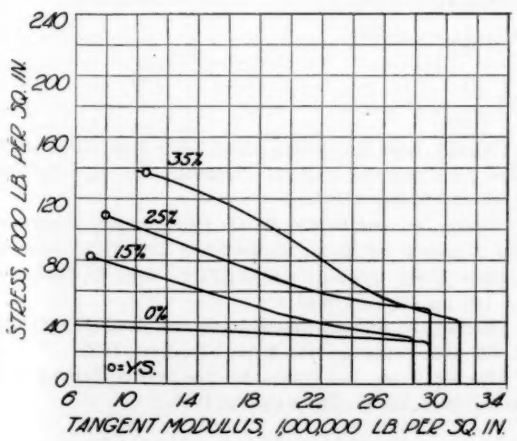

FIG. 13a. Tension, as cold-rolled.

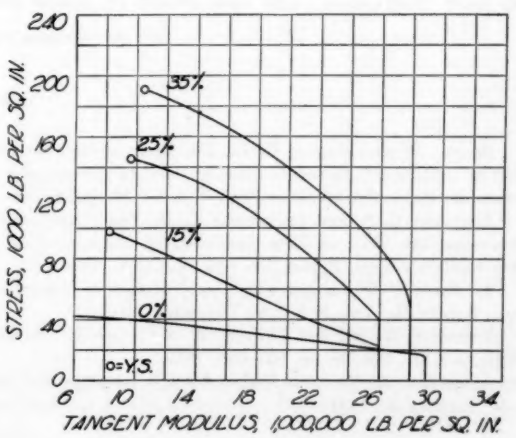

FIG. 13b. Compression, as cold-rolled.

(Figs. 13c and 13d follow on page 432)

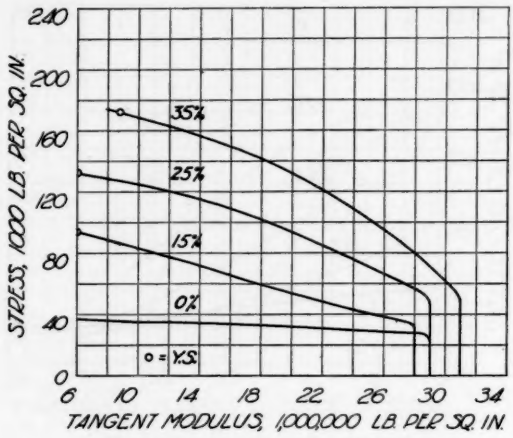

FIG. 13c. Tension, as cold-rolled and heat-treated at 225°C.

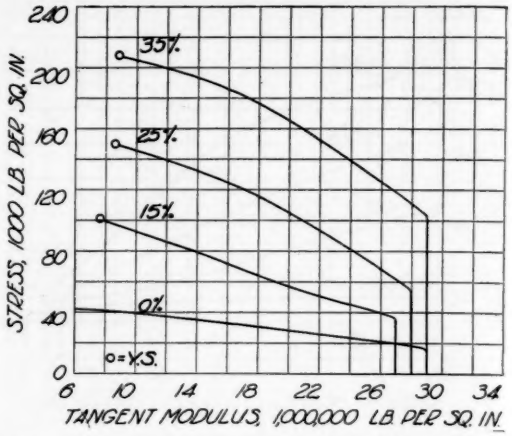

FIG. 13d. Compression, as cold-rolled and heat-treated at 225°C.

FIGS. 13a–13d. Tangent modulus curves derived from stress-strain curves for Steel H194 containing 17.52 per cent chromium, 4.34 per cent nickel, 5.43 per cent manganese, 0.27 per cent silicon, and 0.12 per cent carbon. Transverse to the direction of rolling.

ties are obtained in the cold-rolled chromium-manganese-nickel steels containing 16 to 18 per cent chromium, 5 to 6 per cent manganese, 4 to 5 per cent nickel and 0.10 to 0.16 per cent carbon. In fact, the chromium-manganese-nickel steels have somewhat higher compression properties in the longitudinal direction to rolling than the chromium-nickel steels.

It must not be concluded from what has been said that the fully austenitic cold-rolled steels of the 18 per cent chromium and 8 per cent nickel type are entirely unsuitable for lightweight high-strength service. Steels of this type have satisfactory stress-strain characteristics and good ductility when cold-rolled to tensile strengths as high as about 150,000 lbs. per sq.in. However, as stated previously, when cold-rolled to higher strengths they are likely to be deficient in ductility.

All these steels exhibit different directional properties after cold-rolling, and this should be taken into consideration when the steels are used for lightweight high-strength construction. In compression the yield strength at 0.2 per cent offset is higher in the transverse than in the longitudinal direction to rolling, but in tension the reverse is true. Generally, the yield strength of the chromium-nickel steels at 0.2 per cent offset is higher in tension than in compression in the longitudinal direction to rolling, but in the case of the chromium-manganese-nickel steels the yield strengths in tension and compression in this direction are more nearly equal to each other.

The stress-strain properties of all the steels are improved in both directions to rolling by application of the low-temperature stress-relieving heat-treatment between 200° and 300°C. (392° to 572°F.). The treatment ordinarily consumes a period from a few hours up to about 72 hours, although as a rule maximum improvement is attained in a period of about 24 hours.

(See the following pages for Figs. 14 through 19)

REFERENCES

[1] Franks, R., and Binder, W. O., *The Stress-Strain Characteristics of Cold-Rolled Austenitic Stainless Steel in Compression as Determined by the Cylinder Test Method*, A.S.T.M., June, 1941.

[2] Aitchison, C. S., and Tuckerman, L. B., *The "Pack" Method for Compressive Tests on Thin Specimens of Materials Used in Thin-Wall Structures*, Report No. 649, N.A.C.A., 1939.

[3] Aitchison, C. S., *Extension of "Pack" Method for Compressive Tests*, Report No. 789, N.A.C.A., December, 1940.

[4] Krivobok, V. N., and Lincoln, R. A., *Austenitic Stainless Alloys*, A.S.M., Vol. 25, pp. 637–689, 1937.

[5] Lincoln, R. A., *Stainless Steel in Aircraft*, Iron Age, Vol. 147, p. 35, January 30, 1941.

[6] Bandel, John M., *Stainless Steel; New Data and New Procedure for Comparing Physical Properties*, Iron Age, Vol. 148, pp. 45–52, October 9, 1941.

[7] Franks, R., and Binder, W. O., *Effects of Low Temperature Heat Treatment on Elastic Properties of Cold-Rolled Austenitic Stainless Steels*, Transactions, A.I.M.E., Iron & Steel Div., Vol. 140, pp. 433–458, 1940.

[8] Becket, F. M., *Chromium-Manganese Steels*, Year Book, pp. 173–194; American Iron & Steel Institute, 1930.

[9] Becket, F. M., and Franks, R., *The Book of Stainless Steels*, pp. 497–501; A.S.M., Cleveland, O., 1935.

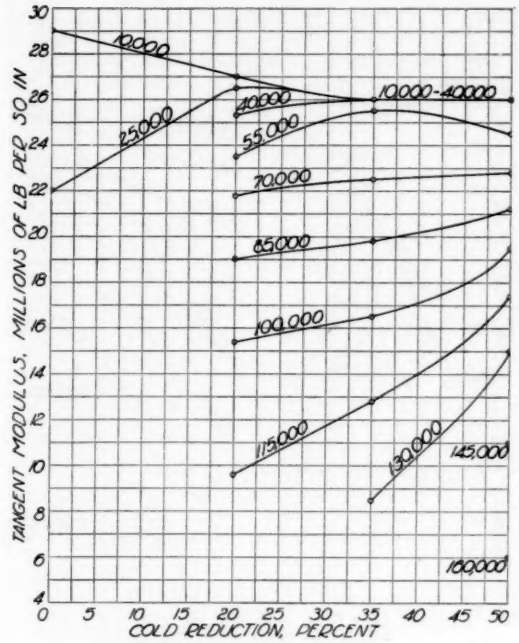

FIG. 14a. Tension, as cold-rolled.

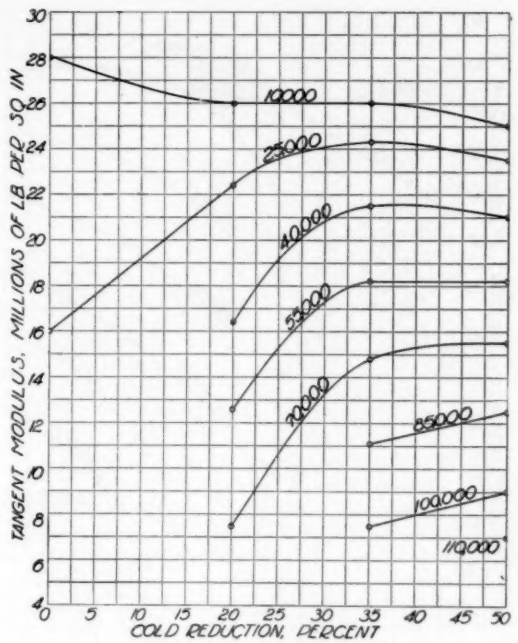

FIG. 14b. Compression, as cold-rolled.

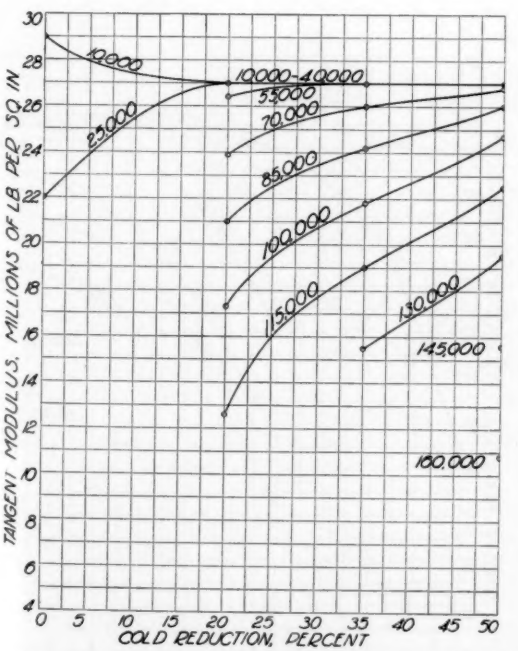

FIG. 14c. Tension, as cold-rolled and heat-treated at 200°C.

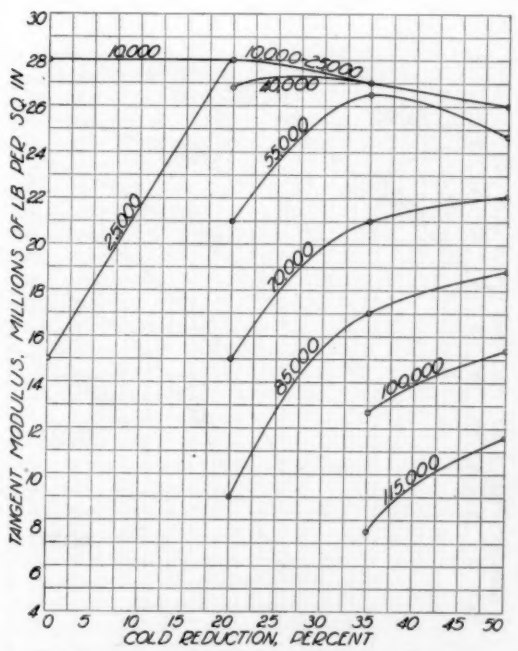

FIG. 14d. Compression, as cold-rolled and heat-treated at 200°C.

FIGS. 14a–14d. Tangent modulus vs. per cent cold reduction at various stress levels. Curves derived from the 18–8 steel data shown in Figs. 3a–3d. Longitudinal to the direction of rolling.

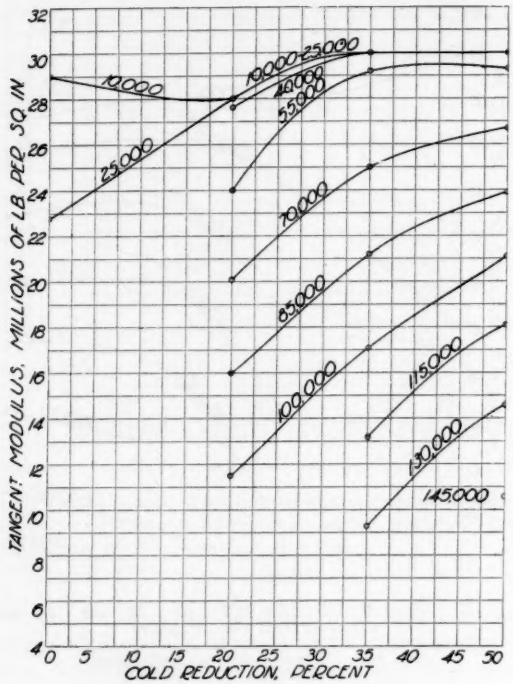

FIG. 15a. Tension, as cold-rolled.

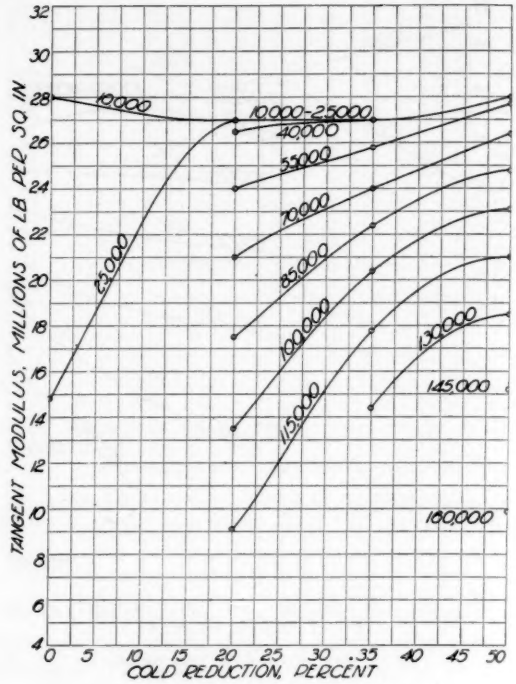

FIG. 15b. Compression, as cold-rolled.

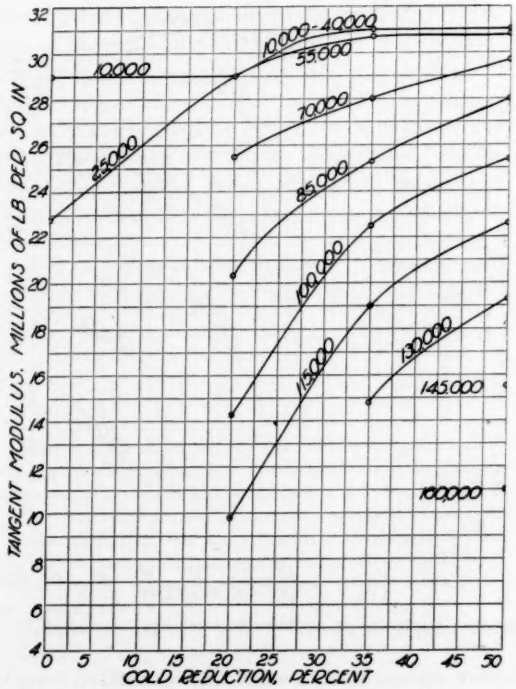

FIG. 15c. Tension, as cold-rolled and heat-treated at 200°C.

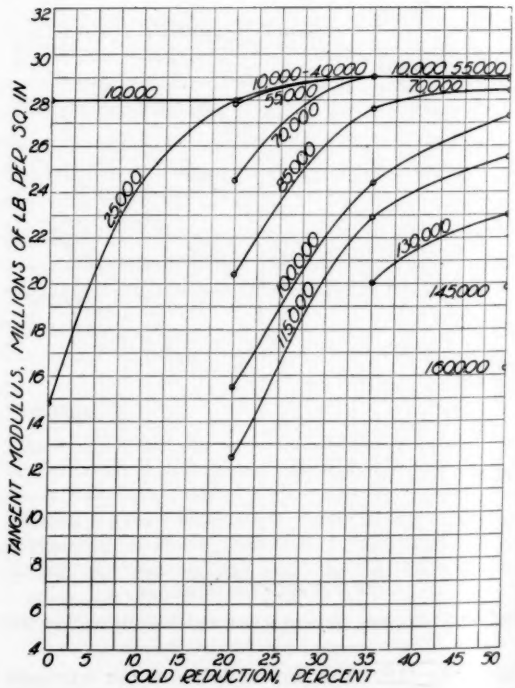

FIG. 15d. Compression, as cold-rolled and heat-treated at 200°C.

FIGS. 15a–15d. Tangent modulus vs. per cent cold reduction at various stress levels. Curves derived from the 18–8 steel data shown in Figs. 4a–4d. Transverse to the direction of rolling.

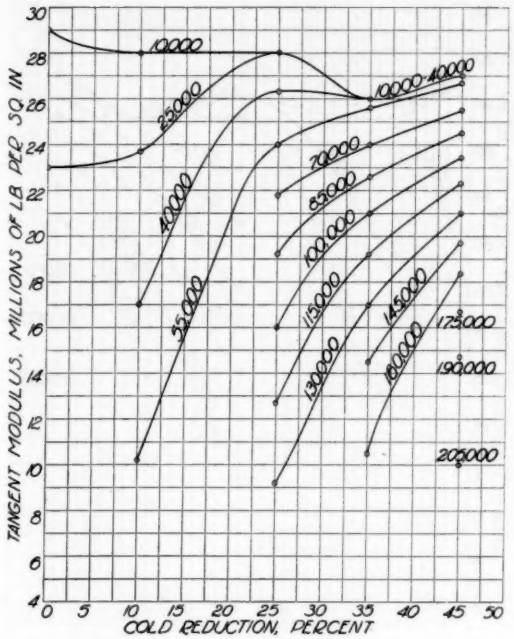

FIG. 16a. Tension, as cold-rolled.

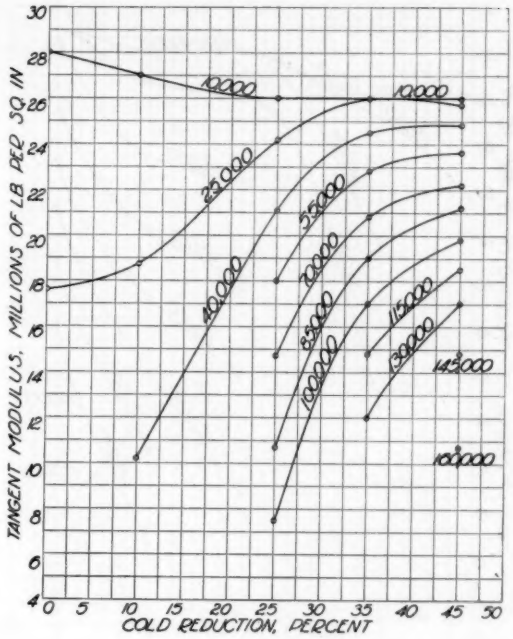

FIG. 16b. Compression, as cold-rolled.

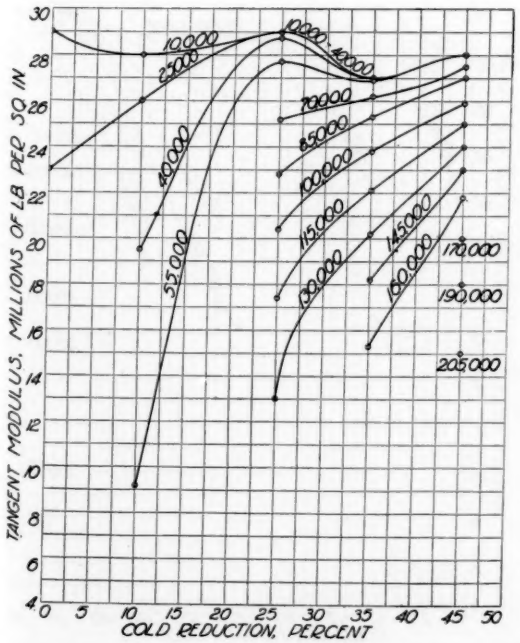

FIG. 16c. Tension, as cold-rolled and heat-treated at 200°–275°C.

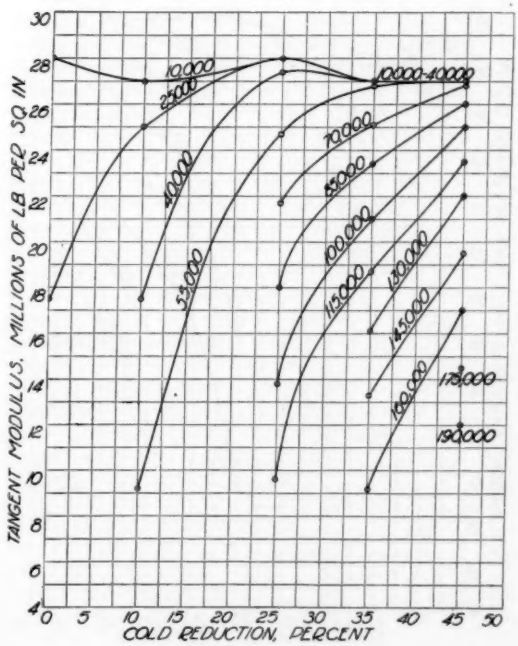

FIG. 16d. Compression, as cold-rolled and heat-treated at 200°–275°C.

FIGS. 16a–16d. Tangent modulus vs. per cent cold reduction at various stress levels. Curves derived from the 17–7 steel data shown in Figs. 8a–8d. Longitudinal to the direction of rolling.

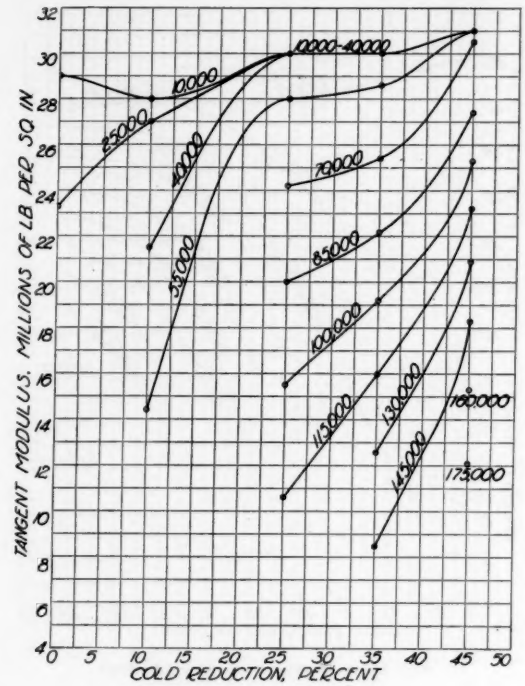

FIG. 17a. Tension, as cold-rolled.

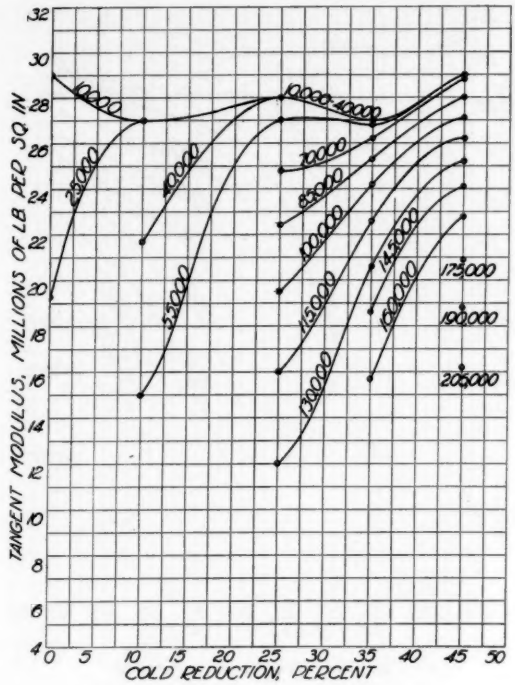

FIG. 17b. Compression, as cold-rolled.

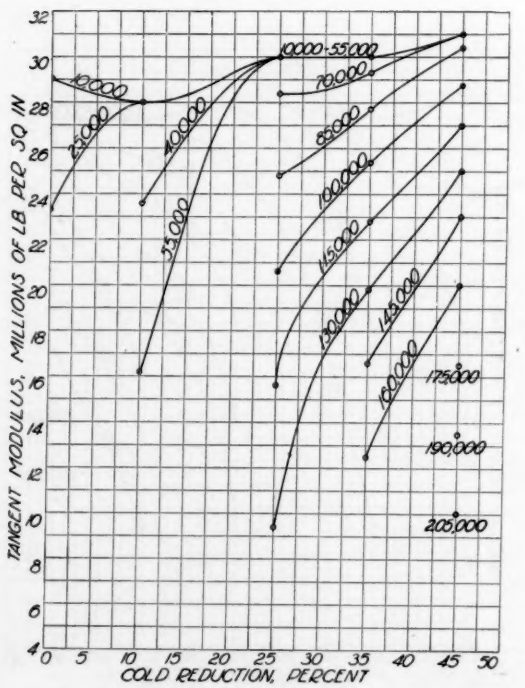

FIG. 17c. Tension, as cold-rolled and heat-treated at 200°–275°C.

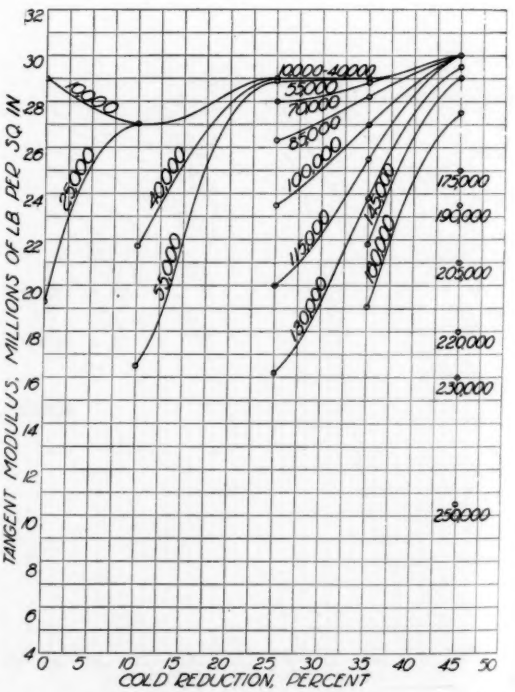

FIG. 17d. Compression, as cold-rolled and heat-treated at 200°–275°C.

FIGS. 17a–17d. Tangent modulus vs. per cent cold reduction at various stress levels. Curves derived from the 17–7 steel data shown in Figs. 9a–9d. Transverse to the direction of rolling.

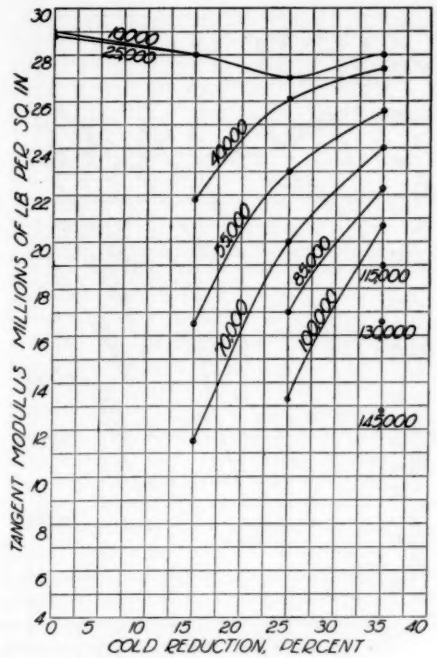

FIG. 18a. Tension, as cold-rolled.

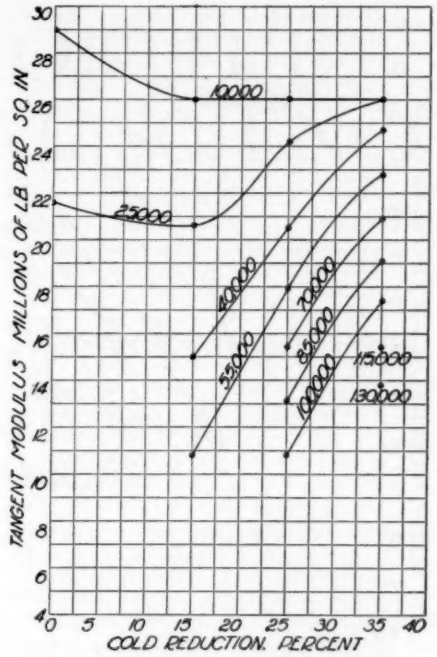

FIG. 18b. Compression, as cold-rolled.

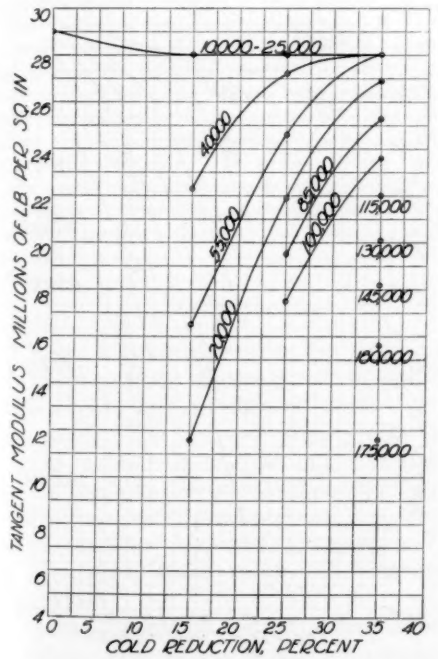

FIG. 18c. Tension, as cold-rolled and heat-treated at 225°C.

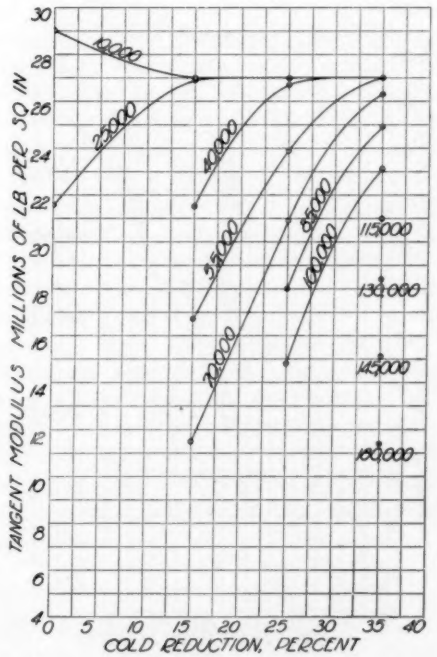

FIG. 18d. Compression, as cold-rolled and heat-treated at 225°C.

FIGS. 18a–18d. Tangent modulus vs. per cent cold reduction at various stress levels. Curves derived from the 17 per cent chromium-5 per cent manganese-4 per cent nickel steel data shown in Figs. 12a–12d. Longitudinal to the direction of rolling.

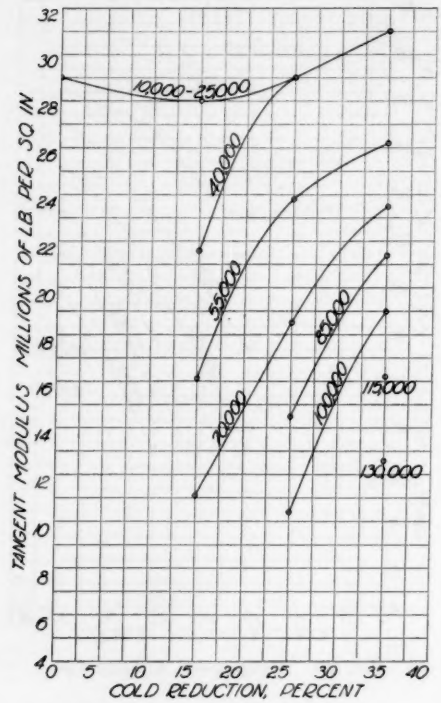

FIG. 19a. Tension, as cold-rolled.

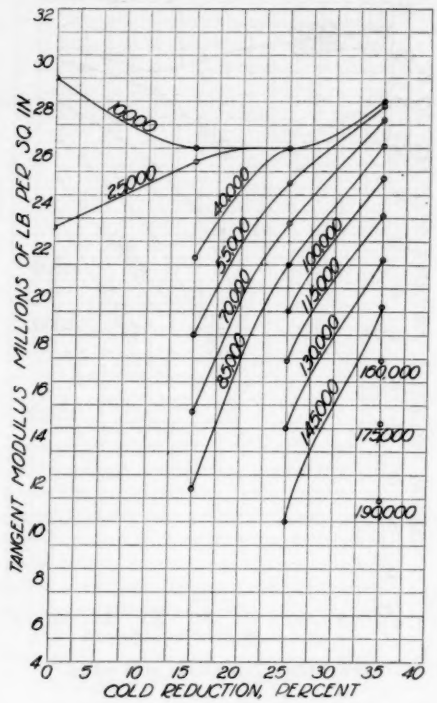

FIG. 19b. Compression, as cold-rolled.

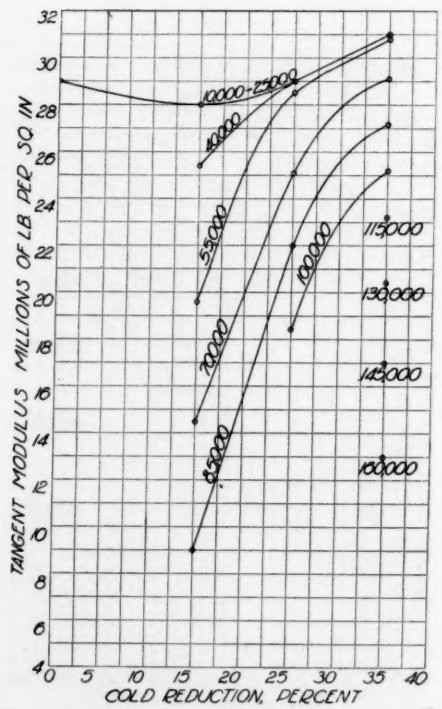

FIG. 19c. Tension, as cold-rolled and heat-treated at 225°C.

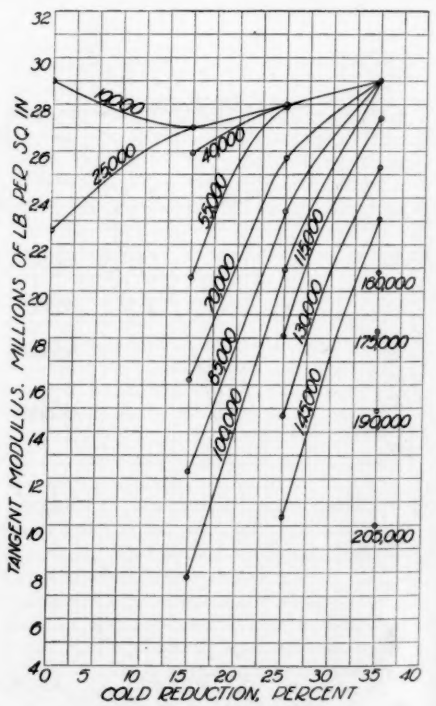

FIG. 19d. Compression, as cold-rolled and heat-treated at 225°C

FIGS. 19a–19d. Tangent modulus vs. per cent cold reduction at various stress levels. Curves derived from the 17 per cent chromium-5 per cent manganese-4 per cent nickel steel data shown in Figs. 13a–13d. Transverse to the direction of rolling.